© 2017. Published by The Company of Biologists Ltd | Development (2017) 144, 2994-3005 doi:10.1242/dev.151712

TECHNIQUES AND RESOURCES

RESEARCH ARTICLE

Genome-wide analysis of facial skeletal regionalization in zebrafish

Amjad Askary*, Pengfei Xu*, Lindsey Barske*, Maxwell Bay, Paul Bump, Bartosz Balczerski, Michael A. Bonaguidi and J. Gage Crump‡

ABSTRACT

Patterning of the facial skeleton involves the precise deployment of thousands of genes in distinct regions of the pharyngeal arches. Despite the significance for craniofacial development, how genetic programs drive this regionalization remains incompletely understood. Here we use combinatorial labeling of zebrafish cranial neural crest-derived cells (CNCCs) to define global gene expression along the dorsoventral axis of the developing arches. Intersection of region-specific transcriptomes with expression changes in response to signaling perturbations demonstrates complex roles for Endothelin 1 (Edn1) signaling in the intermediate joint-forming region, yet a surprisingly minor role in ventralmost regions. Analysis of co-variance across multiple sequencing experiments further reveals clusters of co-regulated genes, with *in situ* hybridization confirming the domain-specific expression of novel genes. We then created loss-of-function alleles for 12 genes and uncovered antagonistic functions of two new Edn1 targets, *follistatin a* (*fsta*) and *emx2*, in regulating cartilaginous joints in the hyoid arch. Our unbiased discovery and functional analysis of genes with regional expression in zebrafish arch CNCCs reveals complex regulation by Edn1 and points to novel candidates for craniofacial disorders.

KEY WORDS: Craniofacial, Zebrafish, Jaw, Skeleton, Cartilage, Bone, Cranial neural crest, Dorsoventral patterning, Endothelin, Edn1, Jagged-Notch, Dlx5a, Hand2, Emx2, Fsta, Mrrf

INTRODUCTION

The vertebrate facial skeleton is generated from cranial neural crest-derived cells (CNCCs) that populate a series of pharyngeal arches (Platt, 1893; Schilling and Kimmel, 1994). Signaling from endodermal and ectodermal epithelia, as well as from CNCCs themselves, establishes nested patterns of gene expression in arch CNCCs, in particular along the dorsoventral axis (Medeiros and Crump, 2012; Mork and Crump, 2015). CNCCs then progressively adopt a number of fates, including cartilage, bone, and ligament (Bronner and LeDouarin, 2012), with a subset of cells remaining as progenitors for later differentiation and possibly adult repair (Paul et al., 2016). The shapes and functions of distinct facial regions are inextricably tied to the selection of these cell fates and the subsequent growth and rearrangements of skeletal cells (Kimmel et al., 1998). The earliest fate adopted by arch CNCCs is cartilage, which occurs first in ventral-intermediate arch regions and then spreads to ventral and dorsal poles (Barske et al., 2016). Domain-specific differences in cartilage versus bone fates are likely to contribute to region-specific skeletal morphologies. In dorsal and intermediate domains, early cartilage differentiation must be actively suppressed to ensure proper formation of joints and later-forming intramembranous bones (Askary et al., 2015; Nichols et al., 2016). Identifying the molecular differences that prefigure regional cell fate choices and behaviors is therefore key to unraveling how the facial skeleton is assembled.

Candidate-based approaches, as well as forward genetic screens in zebrafish (Piotrowski et al., 1996; Schilling et al., 1996), have identified key members of craniofacial signaling pathways and their downstream targets (Minoux and Rijli, 2010). Edn1 signaling is required for gene expression and subsequent skeletal patterning in the intermediate and ventral-intermediate regions of the arches, including the joint-forming domain (Kurihara et al., 1994; Clouthier et al., 1998; Miller et al., 2000; Ozeki et al., 2004; Sato et al., 2008; Gordon et al., 2013). The Bmp pathway has an overlapping function in patterning the lower face (Tucker et al., 1998; Bonilla-Claudio et al., 2012), although it appears to be preferentially required for gene expression in ventralmost arch regions (Alexander et al., 2011; Zuniga et al., 2011). By contrast, Jagged-Notch signaling is required to pattern dorsal arch CNCCs, at least in the hyoid and posterior mandibular arches of zebrafish (Zuniga et al., 2010; Barske et al., 2016). Downstream targets have also been identified, including Edn1 activation and Jagged-Notch inhibition of the Dlx3/4/5/6 family in ventral-intermediate CNCCs (Beverdam et al., 2002; Depew et al., 2002; Talbot et al., 2010; Zuniga et al., 2010), and Edn1 and Bmp regulation of Hand2 in ventral CNCCs (Thomas et al., 1998; Miller et al., 2003; Yanagisawa et al., 2003; Zuniga et al., 2011; Bonilla-Claudio et al., 2012). However, the extent to which Edn1 and Notch globally regulate dorsoventral gene expression remains incompletely understood.

Recently, genome-wide expression profiling in mice has identified stage-specific expression signatures of craniofacial compartments, such as the mandibular, maxillary and frontonasal prominences (Feng et al., 2009; Fujita et al., 2013; Brunskill et al., 2014; Hooper et al., 2017). Similar studies have revealed genes regulated by Bmp4 (Bonilla-Claudio et al., 2012) and Dlx5/6 (Jeong et al., 2008). These studies largely relied on dissection of facial prominences rather than purification of the arch CNCCs that generate the facial skeleton. As the arches consist of not only CNCCs, but also endodermal and ectodermal epithelia and mesodermal cores, whether the identified genes were expressed in CNCCs was not always clear.

In the current study, we use the nested expression of *hand2*:GFP and *dlx5a*:GFP transgenes along the dorsoventral axis to identify genes with domain-specific expression in CNCCs of the zebrafish mandibular and hyoid arches. By combining this domain-specific

Eli and Edythe Broad Center for Regenerative Medicine and Stem Cell Research, University of Southern California, Los Angeles, CA 90033, USA.
*These authors contributed equally to this work

‡Author for correspondence (gcrump@usc.edu)

J.G.C., 0000-0002-3209-0026

Received 7 March 2017; Accepted 10 July 2017

Development (2017) 144, 2994-3005 doi:10.1242/dev.151712

profiling with effects of altered signaling on arch CNCCs (Barske et al., 2016), we demonstrate global roles for Edn1 and Jagged-Notch signaling in establishing intermediate/ventral-intermediate and dorsal arch gene expression, respectively, yet only a minor role for Edn1 in the ventralmost arches. We then used gene editing to test the requirements for 12 previously uncharacterized domain-specific genes and found opposing requirements for two new Edn1 targets, *fsta* and *emx2*, in coordinating skeletal development in the intermediate hyoid arch. Whereas *fsta* inhibits cartilage differentiation in the developing hyoid joint, *emx2* promotes cartilage differentiation at the connection points between individual hyoid cartilages. Thus, in addition to providing a global description of dorsoventral gene expression in arch CNCCs, these findings uncover a complex role for Edn1 in balancing skeletal differentiation in the intermediate arches.

RESULTS

Generation of domain-specific arch transcriptomes by combinatorial transgene labeling

We have previously reported using dual labeling by *sox10*:DsRed and *fli1a*:GFP transgenes to purify all arch CNCCs from embryos at 20, 28, and 36 h post-fertilization (hpf), followed by mRNA isolation, cDNA library construction and deep sequencing (Barske et al., 2016). Here, we performed two additional replicates at 36 hpf to better define a minimum set of 472 arch CNCC-enriched genes. Next, we took advantage of the nested patterns of *hand2*:GFP and *dlx5a*:GFP transgenes to isolate distinct subsets of arch CNCCs along the dorsoventral axis at 36 hpf, followed by RNA sequencing (RNAseq) (Fig. 1A). Whereas fluorescence activated cell sorting (FACS) of *hand2*:GFP^{+}; *sox10*:DsRed^{+} cells enriches for the ventralmost CNCCs of the arches, FACS of *dlx5a*:GFP^{+}; *sox10*:DsRed^{+} cells enriches for a broader domain of ventral to intermediate arch CNCCs (and the otic vesicle).

We then compared how RNAseq data from different experiments align to the zebrafish genome. In our analysis, we included new *hand2*:GFP and *dlx5a*:GFP samples, as well as the previously described *sox10*:DsRed^{+}; *fli1a*:GFP^{+} cells from wild types, *edn1* mutants, *jag1b* mutants, and embryos with elevated Edn1 (*hsp70l*:Gal4; *UAS*:Edn1) and Notch (*hsp70l*:Gal4; *UAS*:Notch1a-ICD) signaling. For each experiment, the majority of reads (~80-90%) could be aligned to a unique position in the zebrafish genome, and the percentage of uniquely aligned reads was independent of the total number of reads for each particular sample (Fig. 1B). The uniformly high percentage of uniquely aligned reads is a positive indication of the quality of the RNAseq data.

Transcriptomic analysis reveals genes differentially enriched in *hand2*:GFP and *dlx5a*:GFP domains

In order to compare gene expression levels between samples, read counts were normalized to yield transcript per million values (TPMs). We identified the set of 472 genes enriched in arch CNCCs by filtering for genes with average TPMs greater than 2 across the three wild-type *fli1a*:GFP^{+}; *sox10*:DsRed^{+} samples at 36 hpf, as well as for those enriched 1.5-fold or higher in double-positive versus single-positive cells (i.e. non-CNCC) (Tables S4 and S5). We then took advantage of the relative levels of *hand2*:GFP and *dlx5a*:GFP to subdivide arch CNCCs into four dorsoventral domains (Fig. 1C). As previously described, *hand2*:GFP displays graded expression from strong in ventralmost domains to weaker in more ventral-intermediate regions, and *dlx5a*:GFP transitions from strong in ventral and intermediate regions to weaker in dorsal

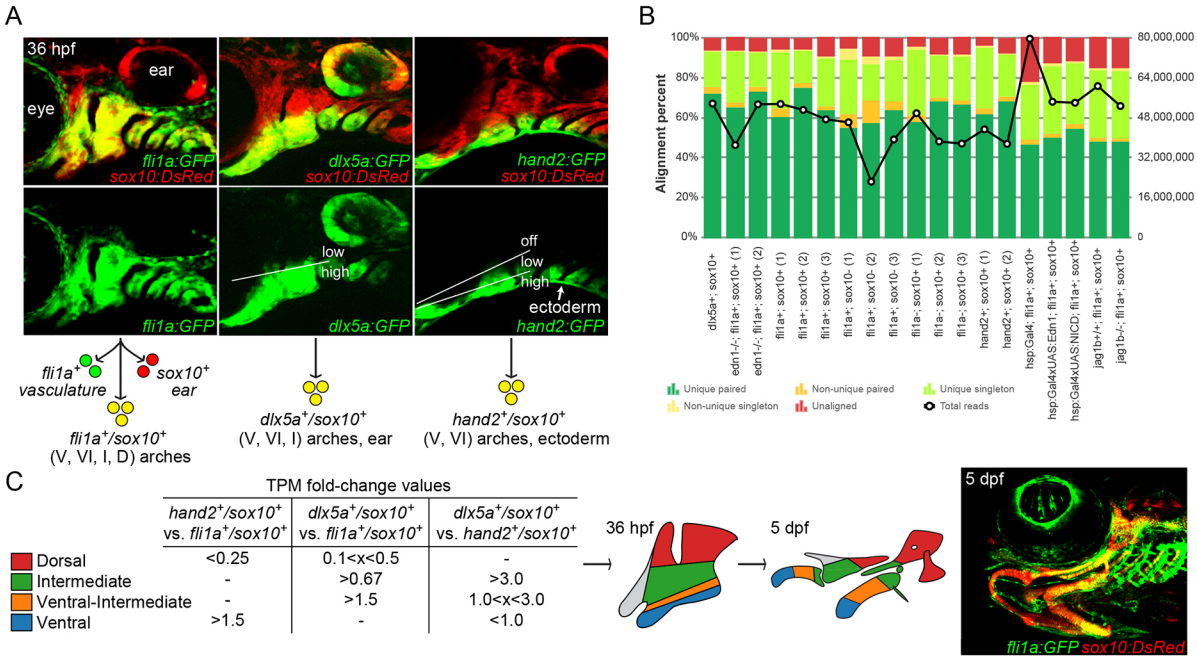

Fig. 1. Isolation of arch CNCCs for RNAseq. (A) Cells were sorted using transgenic lines that label different populations of arch CNCCs. *fli1a*:GFP and *sox10*:DsRed overlap throughout arch CNCCs (yellow); *dlx5a*:GFP and *sox10*:DsRed in CNCCs of ventral (V) to intermediate (I) domains, as well as some dorsal (D) domain CNCCs and the otic vesicle; and *hand2*:GFP and *sox10*:DsRed in ventral and more weakly in ventral-intermediate (VI) CNCCs [modified from Barske et al. (2016) and Medeiros and Crump (2012)]. (B) Breakdown of alignment results for each RNAseq experiment, showing the percentage of reads aligned to a unique site in the genome and whether both paired-end reads were aligned. The line graph shows the total number of reads acquired for each sample. (C) Dorsal, intermediate, ventral-intermediate, and ventral domains were defined by their relative enrichment levels (i.e. fold-change of TPM values) among *hand2*:GFP; *sox10*:DsRed, *dlx5a*:GFP; *sox10*:DsRed, and *fli1a*:GFP; *sox10*:DsRed cells. These domains correspond to specific parts of the arches at 36 hpf that give rise to the larval craniofacial skeleton at 5 dpf (shown for context in a *fli1a*:GFP; *sox10*:DsRed fish).

Development (2017) 144, 2994-3005 doi:10.1242/dev.151712

domains (Medeiros and Crump, 2012). We therefore binned genes into clusters by comparing their relative expression in cells sorted with different transgenes: *hand2*:GFP^{high}; *dlx5a*:GFP^{high} ('ventral', 15 genes), *hand2*:GFP^{low}; *dlx5a*:GFP^{high} ('ventral-intermediate', 22 genes), *hand2*:GFP^{-}; *dlx5a*:GFP^{high} ('intermediate', 16 genes), and *hand2*:GFP^{-}; *dlx5a*:GFP^{low} ('dorsal', 30 genes) (see Fig. 1C, Table 1 for cut-off values). Confirming the validity of this filtering strategy, each dorsoventral cluster includes several genes with known expression in that domain (Table S1). For example, the ventral cluster includes endogenous *hand2* (Miller et al., 2003) and homologs of genes known to be expressed in the ventral/distal domains of the murine arches (*foxf1* and *foxf2a*) (Jeong et al., 2004); the ventral-intermediate cluster includes endogenous *dlx5a*, as well as *dlx3b*, *dlx4b* and *msxe* (*msx1a*) (Miller et al., 2000); the intermediate cluster includes *grem2b* (Zuniga et al., 2011) and genes required for joints such as *irx7* (Askary et al., 2015) and *nkx3.2* (Miller et al., 2003); and the dorsal cluster includes *jag1b* (Zuniga et al., 2010) and homologs of murine genes with dorsal arch expression (*pou3f3a* and *pou3f3b*) (Jeong et al., 2008).

In situ validation of novel domain-specific gene expression in the arches

Given the inclusion of known genes with correctly predicted dorsoventral expression, we sought to validate the expression of uncharacterized genes in each domain-specific list. To do so, we conducted fluorescent *in situ* hybridization in 36 hpf embryos, along with *sox10*:GFPCAAX (membrane GFP) in a second color to highlight all arch CNCCs.

Ventral genes

Of the eight predicted ventral genes tested, all showed some expression in the ventral mandibular or hyoid arches, yet their expression patterns were distinct (Fig. 2A). Similar to *hand2* (Miller et al., 2000), we observed expression of *foxf1*, *foxf2a*, *fzd9b*, *smad6a* and *skp2* in the ventralmost CNCCs of both arches, with *pitx1* showing more limited ventral expression in only the mandibular arch. By contrast, *sema3bl* and *twist1b* were expressed in the ventral domain and also, to a lesser degree, in subsets of dorsal arch CNCCs, reminiscent of the published expression pattern of *barx1* (Nichols et al., 2013; Barske et al., 2016), another gene on our ventral list. The weaker expression of these genes in dorsal relative to ventral arch CNCCs, together with their lower levels in the intermediate domain, is likely to explain why they were enriched in the *hand2*:GFP dataset and classified as ventral genes by our filtering scheme.

Ventral-intermediate genes

Among the predicted ventral-intermediate genes, two out of five tested showed expression within the ventral-intermediate domain (*fgfbp2a* and *shox*), one displayed both ventral-intermediate and some dorsal expression (*stmn1a*), one was expressed in the ventral mandibular arch and dorsal posterior hyoid arch cells (*tmem107l*), and one in intermediate regions (*her6*) (Fig. 2B). The ventral-intermediate list also contains several known genes with apparent arch-wide expression [*hoxa2b* and *hoxb2a* (Hunter and Prince, 2002) and *dlx1a* (Sperber et al., 2008)] or ventral and dorsal expression domains (*gsc*) (Miller et al., 2000), although a closer examination of these previous reports suggests higher ventral-intermediate expression for these genes at 36 hpf.

Intermediate genes

Of the four previously characterized genes on this list, three are expressed in the intermediate joint-forming region and required for joints (*irx7*, *grem2b* and *nkx3.2*) (Miller et al., 2003; Zuniga et al.,

Table 1. Predicted genes with dorsoventral-restricted arch expression

Ventral	Ventral-intermediate		Intermediate	Dorsal	
hand2 ✓^{pub}	*fgfbp2a* ✓	*CABZ01110379.1*^{nt}	*emx2* ✓	*pou3f3a* ✓	*cd248a* ✓
sema3bl ✓+	*dlx4b* ✓^{pub}	*her6* ✗^{int}	*irx7* ✓^{pub}	*prss35*^{nt}	*arl4ca*^{nt}
fzd9b ✓	*dlx3b* ✓^{pub}	*msxe* ✓^{pub}	*si:ch73-166c6.1*^{nt}	*fmoda*^{nt}	*jag1b* ✓^{pub}
foxf2a ✓	*si:dkey-16p21.8*^{nt}	*si:ch211-282k23.2*^{nt}	*fsta* ✓	*si:dkeyp-3b12.6*^{nt}	*zfp36l1b*^{nt}
dcps^{nt}	*hoxa2b* ✗^{pub}	*otud4*^{nt}	*zgc:162612*^{nt}	*sfrp2* ✗^{meso}	*thbs1b*^{nt}
smad6a ✓	*shox* ✓	*hoxb2a* ✗^{pub}	*igfbp5b* ✓	*kera*^{nt}	*s1pr3a*^{nt}
cep57l1^{nt}	*dlx5a* ✓^{pub}	*ift22*^{nt}	*ctgfb* ✓	*emp2*^{nt}	*rassf10a* ✗^{ecto}
foxf1 ✓	*gsc* ✓+^{pub}	*dlx1a* ✓^{pub}	*grem2b* ✓^{pub}	*calhm2*^{nt}	*wu:fb92b05*^{nt}
skp2 ✓	*tmem107l* ✗^{ven}	*id3*^{nt}	*ms4a17a.11*^{nt}	*cdh11* ✓	*osr2* ✗
crabp2b^{nt}	*stmn1a* ✓+	*tmem119b*^{nt}	*foxd1* ✓	*pou3f3b* ✓	*tril*^{nt}
pitx1 ✓	*si:ch211-222l21.1*^{nt}	*AL929378.1*^{nt}	*nkx3.2* ✓^{pub}	*gata3* ✗^{pub}	*cxcl12b*^{nt}
twist1b ✓+			*dlx4a* ✓^{pub}	*serpinf1*^{nt}	*dse*^{nt}
lrrn3^{nt}			*spon2b*^{nt}	*ednraa* ✓^{pub}	*mn1a*^{nt}
sumo3b^{nt}			*si:dkeyp-3b12.10*^{nt}	*emilin1a*^{nt}	*bmp2b*^{nt}
barx1 ✓+^{pub}			*si:dkeyp-3b12.8*^{nt}	*postnb* ✓	*kctd15a* ✓
			rgmd^{nt}		

This table reflects expression in the mandibular and hyoid arches at 36 hpf only. **Ventral** genes were defined as showing TPM values in *hand2*:GFP^{+}; *sox10*:DsRed^{+} cells >1.5-fold versus *fli1a*:GFP^{+}; *sox10*:DsRed^{+} and >1.0-fold (i.e. any detectable increase) versus *dlx5a*:GFP^{+}; *sox10*:DsRed^{+} cells. The rationale was that ventralmost genes would show higher expression in *hand2*:GFP^{+} versus *dlx5a*:GFP^{+} cells. **Ventral-intermediate** genes were defined as TPM values in *dlx5a*:GFP^{+}; *sox10*:DsRed^{+} cells >1.5-fold versus *fli1a*:GFP^{+}; *sox10*:DsRed^{+} and between 1.0- and 3.0-fold greater versus *hand2*:GFP^{+}; *sox10*:DsRed^{+} cells. The rationale was that *hand2*:GFP is present but weaker in the ventral-intermediate domain compared with *dlx5a*:GFP. **Intermediate** genes were defined as TPM values in *dlx5a*:GFP^{+}; *sox10*:DsRed^{+} cells >0.67-fold versus *fli1a*:GFP^{+}; *sox10*:DsRed^{+} and >3.0-fold versus *hand2*:GFP^{+}; *sox10*:DsRed^{+} cells. The rationale was that *dlx5a*:GFP only partially overlaps, and *hand2*:GFP not at all, with the intermediate domain. **Dorsal** genes were defined as TPM values in *fli1a*:GFP^{+}; *sox10*:DsRed^{+} cells >4.0-fold versus *hand2*:GFP^{+}; *sox10*:DsRed^{+} and between 2.0- and 10.0-fold greater versus *dlx5a*:GFP^{+}; *sox10*:DsRed^{+}. The rationale was that *hand2*:GFP and *dlx5a*:GFP have little to no expression in the dorsal domain. However, we noted that genes greater than 10.0-fold enriched versus *dlx5a*:GFP included several with known frontonasal expression (e.g. *alx1* and *pitx2*). As the more anterior frontonasal domain has no *dlx5a*:GFP expression, we therefore excluded genes with greater than 10.0-fold enrichment versus *dlx5a*:GFP. ✓, positive expression in predicted domain; ✓+ , positive expression in predicted domain as well as other domains; ✗, expression outside the predicted domain; ven, expression in the ventral domain; int, expression in the intermediate domain; meso, expression in mesoderm; ecto, expression in ectoderm; pub, previously published; nt, not tested.

Development (2017) 144, 2994-3005 doi:10.1242/dev.151712

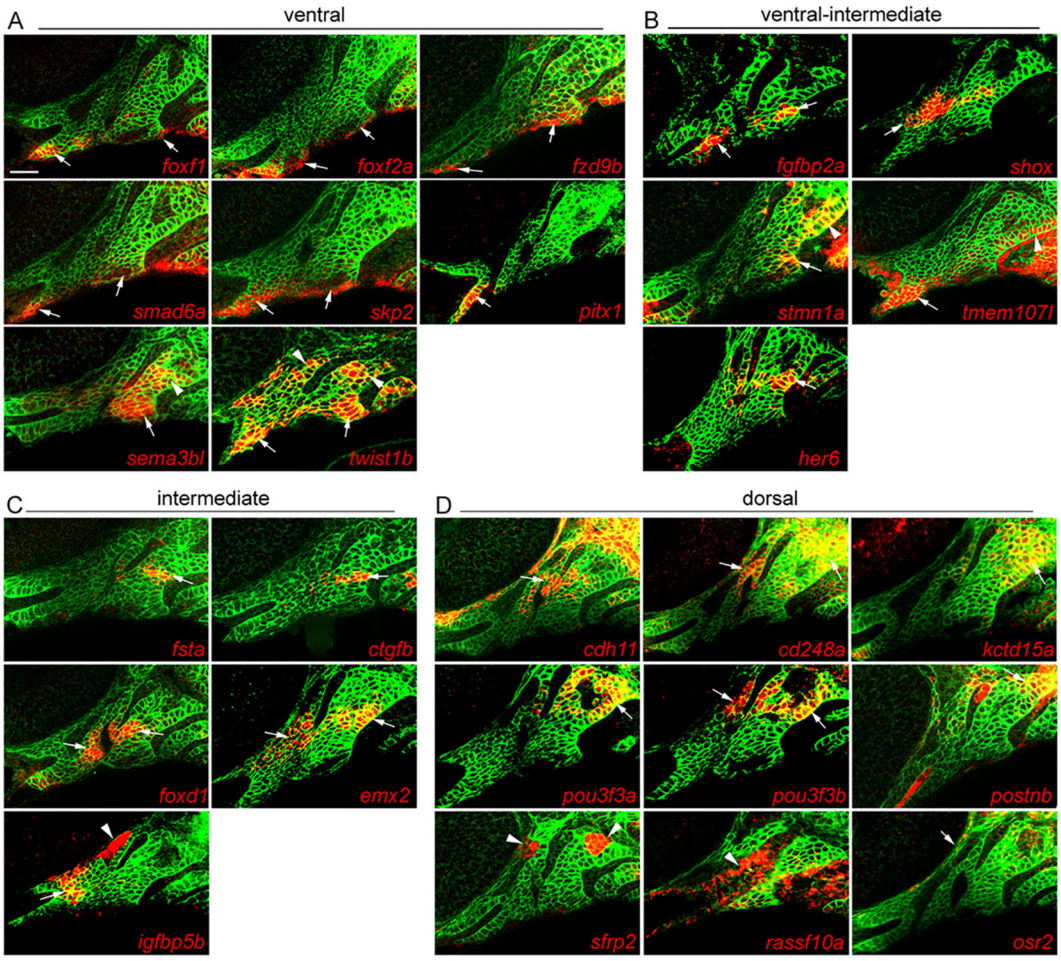

Fig. 2. Arch expression of predicted domain-specific genes. Whole-mount fluorescent *in situ* hybridizations for select genes were performed in *sox10*:GFPCAAX embryos at 36 hpf, with anti-GFP staining (green) showing CNCCs of the mandibular and hyoid arches. (A) *foxf1*, *foxf2a*, *fzd9b*, *smad6a* and *skp2* are expressed in ventral domains of both arches, *pitx1* only in the ventral mandibular arch, and *sema3bl* and *twist1b* in ventral and dorsal CNCCs. (B) *fgfbp2a* and *shox* are expressed in ventral-intermediate CNCCs, *stmn1a* in ventral-intermediate and dorsal CNCCs, *tmem107l* in ventral mandibular and posterior dorsal hyoid arches, and *her6* in a more dorsal domain. (C) *fsta*, *ctgfb*, *foxd1*, *emx2* and *igfbp5b* show specific intermediate domain expression; *igfbp5b* is also expressed in arch mesoderm. (D) *cdh11*, *cd248a*, *kctd15a*, *pou3f3a*, *pou3f3b* and *postnb* are expressed in dorsal CNCCs, *sfrp2* in dorsal arch mesoderm, *rassf10a* in epithelia, and *osr2* between the dorsal first arch and eye. Arrows point to expression in predicted domains, and arrowheads to other arch domains. Single optical sections are shown. Scale bar: 20 µm.

2011; Askary et al., 2015). The inclusion of *dlx4a* might reflect the broader expression of Dlx3-6 genes in both ventral-intermediate and intermediate domains (Talbot et al., 2010), although other members of this family were filtered into the ventral-intermediate category. All five newly tested genes showed highly specific expression in the intermediate domain, including *fsta*, *igfbp5b*, *ctgfb* and homologs of mouse genes expressed in intermediate arch regions – *emx2* (Compagnucci et al., 2013) and *foxd1* (Jeong et al., 2004) (Fig. 2C). Interestingly, *fsta* and *ctgfb* were largely restricted to the hyoid arch and *igfbp5b* to the mandibular arch.

Dorsal genes

We found six of nine predicted dorsal genes to be enriched in the dorsal mandibular and hyoid arches: *cadherin 11* (*cdh11*), *pou3f3a* and *pou3f3b* [homologs of mouse *Pou3f3* with dorsal expression (Jeong et al., 2008)], *cd248a*, *kctd15a* (see also Gharbi et al., 2012) and *postnb* (Fig. 2D). The other three genes were excluded from the *dlx5a*:GFP and *hand2*:GFP expression domains, as predicted, but they did not present typical 'dorsal' expression patterns: *sfrp2* showed dorsal-specific expression but in mesoderm, *rassf10a* was largely confined to the surface ectoderm rather than arch CNCCs, and *osr2* was expressed in a few cells between the mandibular arch and the eye (Swartz et al., 2011). Although not tested here, previous reports also suggest dorsal-enriched expression of *ednraa* from 28-36 hpf (Nair et al., 2007; Zuniga et al., 2010) and expression of *gata3* in the more anterior maxillary prominence (Sheehan-Rooney et al., 2013b).

Distinct regulation of domain-specific genes by Edn1 and Jagged-Notch signaling

Given their major roles in dorsoventral arch patterning, we next tested how Edn1 and Jagged-Notch signaling regulate bulk expression of genes in the dorsoventral domains defined by our RNAseq analysis. We intersected our previously published RNAseq data of gain or loss of Edn1 or Jagged-Notch signaling in arch CNCCs (Barske et al., 2016) with domain-specific genes identified based on enrichment in sorted *hand2*:GFP and *dlx5a*:GFP cells. We found that the expression of intermediate and ventral-intermediate genes, but not ventral and dorsal genes, was significantly reduced in *edn1*$^{-/-}$ embryos (Fig. 3A) and increased

Development (2017) 144, 2994-3005 doi:10.1242/dev.151712

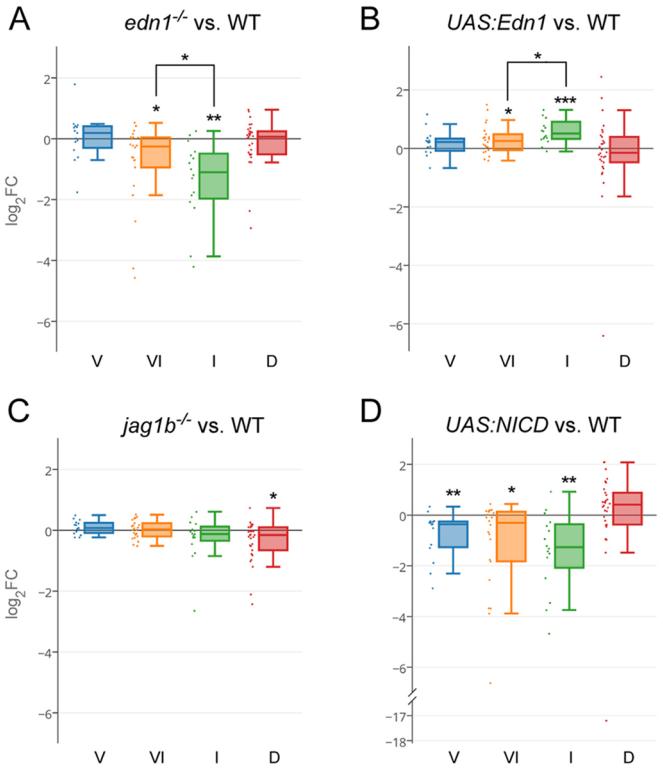

Fig. 3. Domain regulation by Edn1 and Jagged-Notch signaling. (A) In *edn1*$^{-/-}$ mutants, intermediate (I) domain genes are those most strongly downregulated, followed by ventral-intermediate (VI) genes. Ventral (V) and dorsal (D) genes are, on average, unaffected. (B) Edn1 overexpression results in greater upregulation of intermediate than ventral genes. (C) Dorsal genes are downregulated in *jag1b*$^{-/-}$ mutants. (D) Overexpression of the Notch intracellular domain (NICD) downregulates ventral, ventral-intermediate, and intermediate genes. See the Materials and Methods for details of statistical analysis. **P*<0.05, ***P*<0.01, ****P*<0.001.

upon Edn1 misexpression (Fig. 3B). In particular, intermediate genes were most affected by perturbation of Edn1 signaling, consistent with the sensitivity of intermediate skeletal elements (joints, symplectic, palatoquadrate) to partial reduction of Edn1 signaling in zebrafish (Miller and Kimmel, 2001). By contrast, loss of Jagged-Notch signaling in *jag1b*$^{-/-}$ embryos resulted in a downregulation of only dorsal genes (Fig. 3C), and gain of Notch signaling resulted in a downregulation of ventral, ventral-intermediate and intermediate genes (Fig. 3D). Gain of Notch signaling also showed a trend towards increasing the expression of dorsal genes (Bonferroni corrected *P*=0.18).

We next used *in situ* hybridization to confirm the predicted regulation of a subset of genes by Edn1 and Jagged-Notch signaling (Fig. 4). Ventral-intermediate genes *fgfbp2a*, *shox* and *stmn1a*, and intermediate genes *fsta* and *ctgfb*, were reduced in *edn1* mutants. However, the intermediate gene *igfbp5b* was unaffected and the intermediate gene *emx2* was variably upregulated or downregulated in *edn1* mutants. Consistent with RNAseq data, ventral genes *smad6a*, *skp2* and *fzd9b* were unaffected, and the ventral but not dorsal expression of *sema3b1* and the mandibular-specific ventral expression of *pitx1* were lost in *edn1* mutants. Of the dorsal genes examined, *pou3f3a* and *pou3f3b* were ventrally expanded in *edn1* mutants, *cdh11* expression shifted ventrally, and *cd248a* was largely unaffected. Reciprocally, *pou3f3a*, *pou3f3b* and *cd248a* were reduced in *jag1b* mutants, with *cdh11* and *kctd15a* expression unaffected. In summary, we find intermediate and ventral-intermediate genes, but only a subset of ventral and dorsal genes, to be regulated by Edn1 signaling, and a subset of dorsal genes to be regulated by Jagged-Notch signaling.

Co-expression network analysis of pharyngeal arch genes

As an independent strategy to uncover genes co-expressed in arch domains, we performed a weighted gene co-expression network analysis (WGCNA) (Zhang and Horvath, 2005) across 19 of our RNAseq datasets (see Fig. 1B). We limited this analysis to the 6000 genes exhibiting the greatest variance across all datasets and showing an expression level above 2 TPM in at least one experiment. A searchable dendrogram (Fig. S5) reflects the topological overlap metric (TOM), which is a measure of the correspondence in expression between genes across samples. In order to determine the utility of TOM in uncovering novel genes within known networks, we examined five representative branches containing genes with validated dorsoventral-restricted expression (Fig. 5A). Cluster 1 is composed of six genes, including the known dorsal gene *jag1b* (Zuniga et al., 2010). Of these, *cd248a*, *fgf20b* and *snail1a* (*snai1a*) were detected in dorsal arch CNCCs (Fig. 2D, Fig. 5B). Cluster 2 contains 14 genes, including a known intermediate gene (*grem2b*) required for joint formation in zebrafish (Zuniga et al., 2011), as well as four newly validated intermediate genes (*emx2*, *fsta*, *igfbp5b*, *foxd1*) (Fig. 2C). This cluster also contains *twist1a*, which displays more complex expression in dorsal and ventral arch domains (Germanguz et al., 2007). Cluster 3 contains 11 genes, including five tightly clustered Dlx genes (*dlx3b*, *dlx4a*, *dlx4b*, *dlx5a*, *dlx6a*) known to be co-expressed in the ventral-intermediate domain (Talbot et al., 2010), as well as another known ventral-intermediate gene (*msxe*) (Miller et al., 2000) and a non-coding RNA (*si:ch673-351f10.4*) in an analogous position to the mouse *Evf2* (*Dlx6os1*) gene, an antisense transcript that promotes the expression of the *Dlx5-6* locus (Feng et al., 2006). This cluster also contains an uncharacterized gene, *fgfbp2b*, which we find to be expressed in a subset of ventral-intermediate first arch CNCCs (Fig. 5B). We also examined two distinct branches containing ventral-restricted genes. We verified five out of six genes in cluster 4 as being restricted to the ventralmost arches (*pitx1*, *fzd9b*, *foxf1*, *foxf2a*) or expressed more strongly in the ventral arches (*sema3bl*) (Fig. 2A). Cluster 5 contains a known ventral-restricted gene (*satb2*) (Sheehan-Rooney et al., 2013a) that tightly co-varies with *mrrf*, which we find to have similar ventral-restricted expression (Fig. 5B).

We next asked which RNAseq experiments informed gene co-regulation by iteratively computing the average TOM disruption caused by removing experimental groups, thus producing a TOM driver score for each experiment (Fig. 5C). Expression in *dlx5a*:GFP^{+} cells was the strongest driver for cluster 2, containing known and validated intermediate genes, and a strong driver for cluster 3, containing ventral-intermediate-restricted genes. By contrast, expression in *hand2*:GFP^{+} cells was the strongest driver for clusters 4 and 5, consistent with these clusters containing known and newly validated ventral-restricted genes. Consistently, the ventral-intermediate (3) and intermediate (2) clusters and the two ventral clusters (4 and 5) formed separate subgroups when compared across all experiments. By contrast, the dorsal cluster (1) was driven by gain-of-function Notch signaling and not relative enrichment in *dlx5a*:GFP^{+} and *hand2*:GFP^{+} cells. Interestingly, expression in *edn1* mutants was a strong driver for the ventral-intermediate cluster 3, yet disrupted intermediate cluster 2 and ventral cluster 4. This finding is consistent with our *in situ* validation showing opposite Edn1 regulation of intermediate genes *emx2* and

Development (2017) 144, 2994-3005 doi:10.1242/dev.151712

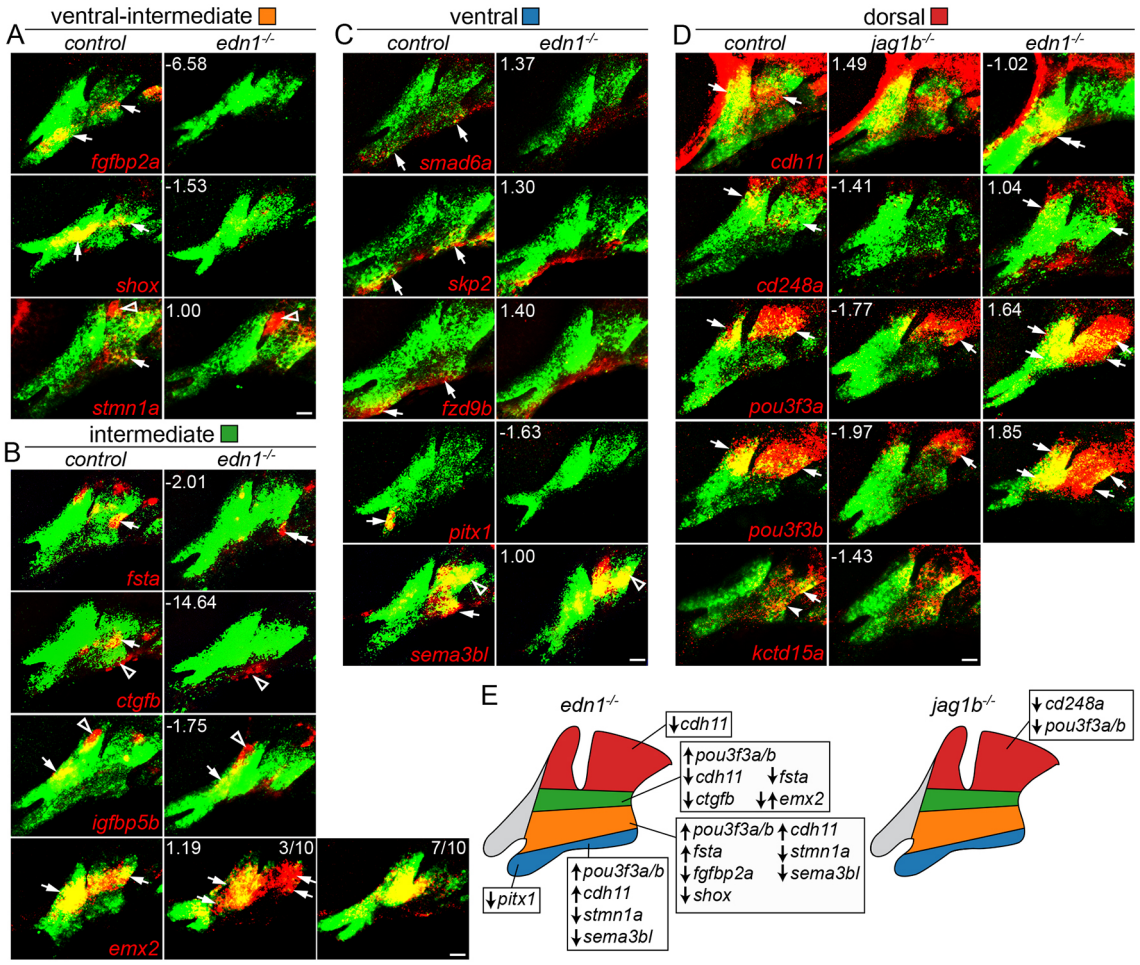

Fig. 4. Changes in domain-specific gene expression in *edn1* and *jag1b* mutants. Two-color fluorescent *in situ* hybridizations were performed for genes of interest (red) and *dlx2a* (green) to label arch CNCCs at 36 hpf. Numbers indicate the gene expression fold-change in mutant versus wild-type *fli1a*:GFP^{+}; *sox10*:dsRed^{+} CNCCs as determined by RNAseq. Maximum intensity projections show the mandibular (left) and hyoid (right) arches. (A) The ventral-intermediate expression of *fgfbp2a*, *shox* and *stmn1a* is lost in *edn1* mutants, yet pouch expression of *stmn1a* is unaffected. (B) In *edn1* mutants, intermediate expression of *fsta* and *ctgfb* is lost, *emx2* is variably upregulated or downregulated, and CNCC and mesoderm expression of *igfbp5b* is unaltered. We also note some ectopic ventral hyoid *fsta* expression in *edn1* mutants. (C) Ventral expression of *smad6a*, *skp2* and *fzd9b* is normal in *edn1* mutants, yet ventral expression of *pitx1* and *sema3bl* is lost. Note that dorsal expression of *sema3bl* is unaffected. (D) In *jag1b* mutants, dorsal expression of *cd248a* is lost, *pou3f3a* and *pou3f3b* are reduced, and *cdh11* and *kctd15a* are unaffected. In *edn1* mutants, *cdh11* expression shifts to ventral CNCCs, *pou3f3a* and *pou3f3b* are ectopically expressed in ventral CNCCs, and *cd248a* is largely unaffected. Arrows indicate expression in predicted arch domains, open arrowheads indicate additional expression domains, and double arrows show expansion into other CNCC domains in mutants. Unless stated otherwise, consistent expression patterns were seen in a minimum of three wild types and three mutants for each experiment. Scale bars: 20 µm. (E) Summary of verified gene expression changes in *edn1* and *jag1b* mutants. Unaffected genes are not listed.

fsta in cluster 2, and regulation of *sema3bl* and *pitx1* but not *fzd9b* in cluster 4. TOM driver analysis thus represents a powerful method for understanding how sets of genes share common expression domains and/or regulation by distinct signaling pathways in the developing face.

We also applied WGCNA to our filtered dorsoventral lists to help resolve false positives (Fig. S1). For genes whose expression patterns were validated by *in situ* hybridization (Fig. 2), 8/8 ventral, 3/3 ventral-intermediate, 4/5 intermediate and 6/6 dorsal genes clustered together on distinct branches. The one outlier was *ctgfb*, although repeating WGCNA without Edn1-related RNAseq datasets revealed that this was due in part to stronger regulation by Edn1 signaling. This analysis also revealed two classes of ventral-intermediate genes: those with more restricted ventral-intermediate expression (similar to the Dlx3-6 class) and those with dual ventral-intermediate and dorsal domains (e.g. *sema3bl* and *twist1b*). We also found that 4/5 genes identified as false positives (*her6*, *osr2*, *tmem107l*, *rassf10a*) did not cluster with other genes in their predicted dorsoventral domains. The sole exception was *sfrp2*, which clustered with dorsal genes despite *in situ* validation revealing expression in dorsal mesoderm and not CNCCs. Thus, combining dorsoventral filtering and WGCNA analysis decreased the false positive rate and uncovered distinct classes of arch expression patterns.

Absence of larval skeletal defects in loss-of-function mutants for many domain-specific genes

We next sought to uncover potential requirements for novel domain-specific genes in zebrafish craniofacial development. We used TALEN and CRISPR technologies to introduce early frameshift mutations in 12 genes (*cd248a*, *ctgfa*, *ctgfb*, *cdh11*, *emx2*, *fsta*, *fstb*, *her6*, *mrrf*, *sfrp2*, *osr1*, *osr2*; see Table S2 for details) and analyzed homozygous mutant embryos for cartilage and bone defects at 5 days post-fertilization (dpf). For all mutants except *fsta* and *emx2*,

Development (2017) 144, 2994-3005 doi:10.1242/dev.151712

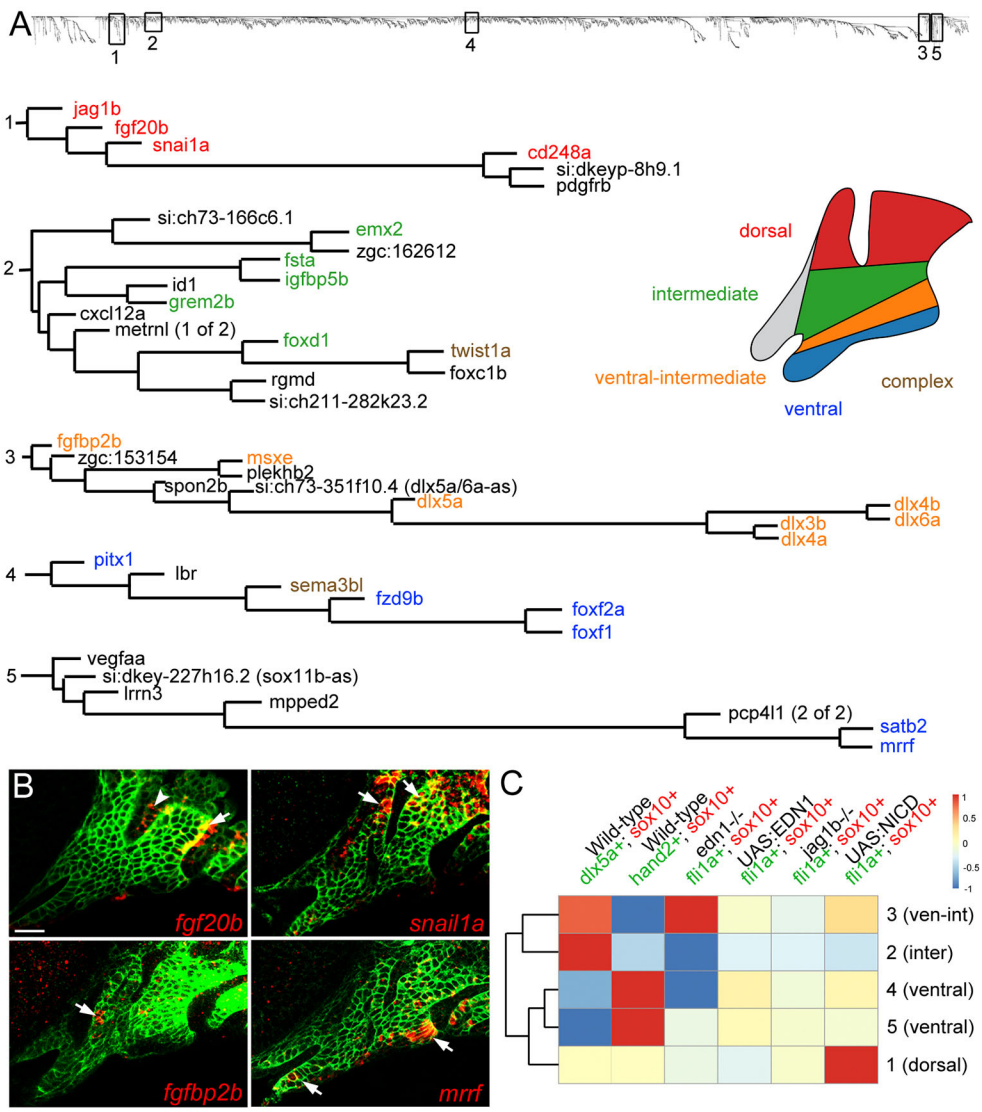

Fig. 5. Co-variance network analysis reveals cohorts of similarly regulated arch genes. (A) Five representative clusters (1-5) were chosen from the dendrogram (top) generated by co-variance analysis. Gene names are color-coded based on expression patterns that are published or verified in this study. 'Complex' refers to genes with broader expression in multiple domains. (B) Four genes discovered by co-variance analysis were confirmed by *in situ* hybridization (red) of *sox10*:GFPCAAX embryos at 36 hpf; anti-GFP staining (green) marks CNCCs of the mandibular and hyoid arches. Arrows indicate CNCC expression and the arrowhead indicates *fgf20b* expression in the first pharyngeal pouch. Scale bar: 20 µm. (C) TOM driver array analysis (see Materials and Methods) shows experiments that drove clustering (red) or disrupted clustering (blue). The dendrogram on the left shows the relatedness of clusters based on which datasets drove their clustering.

no craniofacial skeletal defects were observed (data not shown). *ctgfa; ctgfb* and *osr1; osr2* double mutants also failed to display obvious craniofacial skeletal defects. Although not displaying larval craniofacial defects, *mrrf* mutants grew more slowly than wild-type siblings, rarely survived past 1 month and, even before general growth defects were apparent, were unable to regenerate their tail fins (Fig. S2).

Opposite requirements for *fsta* and *emx2* in hyoid cartilage development

Homozygous mutants for *fsta* and *emx2*, two new Edn1 targets expressed in the intermediate domain, displayed defects in the hyoid arch skeleton (Fig. 6A,B). In *fsta* mutants, we detected variable alterations of the hyoid joint, a compound joint in which a small interhyal cartilage makes connections to the hyomandibular and ceratohyal cartilages on either side. The interhyal cartilage was reduced and made abnormal cartilaginous connections with adjacent cartilages, the symplectic cartilage was reduced in length, and the connection between the hyomandibular and symplectic cartilages was thickened. *fsta; fstb* double mutants displayed a subtle enhancement of craniofacial defects compared with *fsta* single mutants (Fig. S3). These joint and symplectic phenotypes are similar to those reported for *irx7; irx5a* mutants (Fig. 6A) (Askary et al., 2015), and we correspondingly observed a reduction in arch *irx7* expression in 2/7 *fsta; fstb* mutants (Fig. 6E).

By contrast, *emx2* mutants had separated symplectic and hyomandibular cartilages, with weakly Alcian Blue-positive cells evident at the interface. As these two elements start out separate in wild types at 3 dpf (Fig. 6A), we interpret the *emx2* phenotype as a failure of later cartilage fusion. These mutants also have a near complete loss of the opercle bone (a hyoid arch derivative) and abnormalities in the palatoquadrate cartilage (a mandibular arch derivative). The expression of *fsta* and *irx7* is unaffected in *emx2* mutants, and *emx2* expression is unaffected in *fsta* mutants (Fig. 6C-E). Further, loss of *emx2* did not restore normal hyoid joint formation to *fsta* or *irx7; irx5a* mutants, and, conversely, loss of *fsta* or *irx7* and *irx5a* failed to rescue the opercle bone loss of *emx2* mutants (Fig. 6A,B). *fsta* and *emx2*, two intermediate domain genes regulated in distinct ways by Edn1, therefore act in parallel pathways, with *fsta* acting upstream of *irx7* to promote early joint and symplectic formation and *emx2* promoting later cartilage fusion and bone development (Fig. 6F).

DISCUSSION

Our global gene expression analysis of zebrafish pharyngeal arch CNCCs revealed general principles of arch patterning and novel

Development (2017) 144, 2994-3005 doi:10.1242/dev.151712

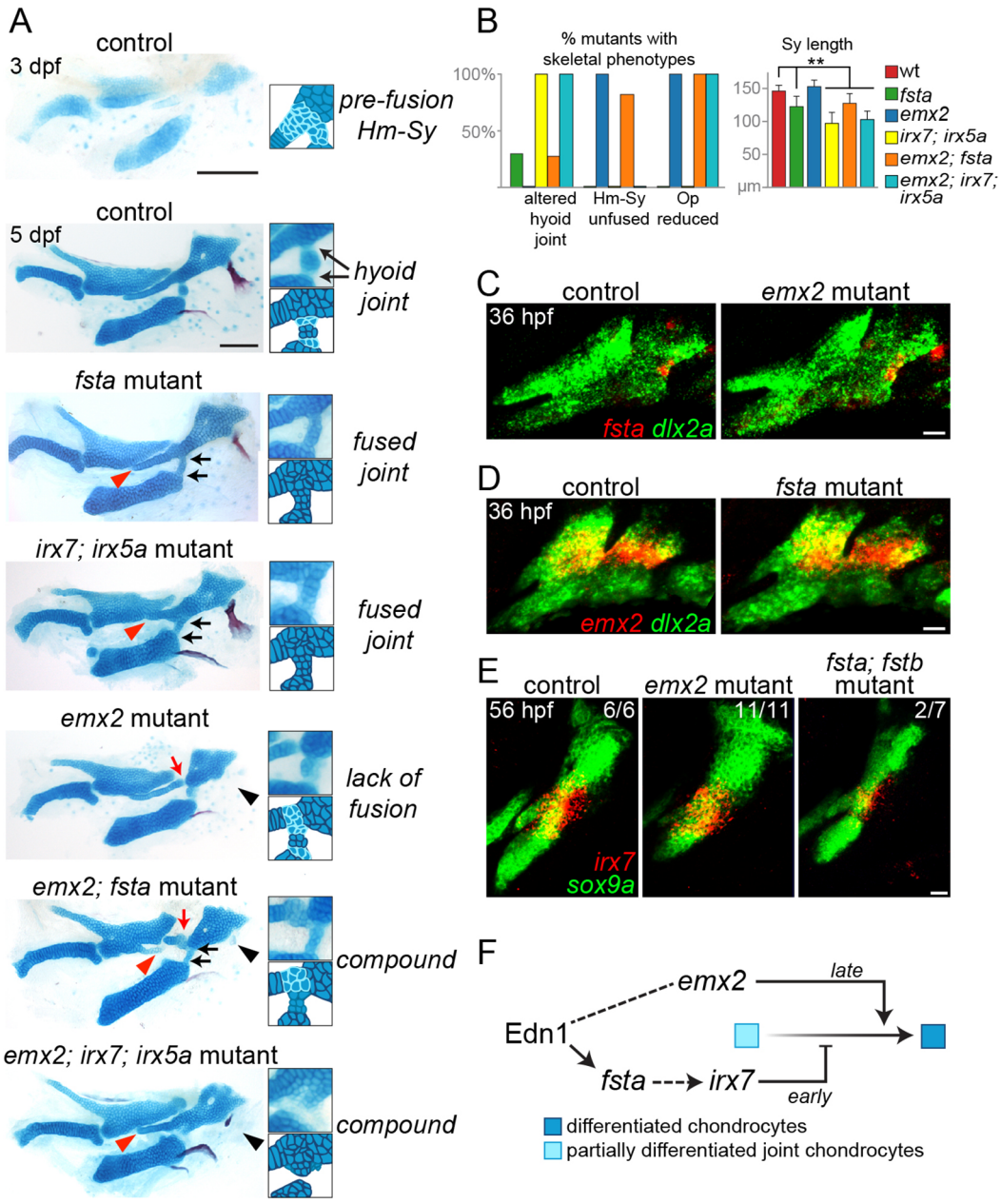

Fig. 6. Distinct roles of Fsta and Emx2 in hyoid skeletal development. (A) Dissected mandibular and hyoid skeletons stained with Alcian Blue (cartilage) and Alizarin Red (bone). At 3 dpf, cells between the hyomandibular (Hm) and symplectic (Sy) cartilages and at the forming hyoid joint region stain weakly with Alcian Blue, reflecting their chondrogenic immaturity. By 5 dpf, rearrangements among cells at the Hm-Sy junction result in elongation of Sy, and maturation of cells at the junction fuses Hm and Sy. Cells in the hyoid joint remain immature and weakly Alcian Blue positive. In *fsta* mutants, the Sy is shortened (red arrowhead), with a build up of chondrocytes in the Hm-Sy junction, and hyoid joint cells inappropriately mature into chondrocytes strongly stained by Alcian Blue, fusing the joint (black arrows). These phenotypes are similar to those of *irx7; irx5a* mutants. In *emx2* mutants, the Hm and Sy cartilages fail to fuse completely (red arrow), and the opercle bone is lost (black arrowhead). *emx2; fsta* mutants show a compound phenotype, including hyoid joint fusion and reduction of Sy. Hm and Sy are disconnected in *emx2; fsta* but not *emx2; irx7; irx5a* mutants. Scale bars: 100 µm. (B) Penetrance of skeletal phenotypes in each genotype: *n* (sides)=57 ($fsta^{-/-}$), 42 ($emx2^{-/-}$), 5 ($irx7^{-/-}$; $irx5a^{-/-}$), 11 ($emx2^{-/-}$; $fsta^{-/-}$) and 7 ($emx2^{-/-}$; $irx7^{-/-}$; $irx5a^{-/-}$). $^{**}P<0.01$ versus wild type. (C,D) Two-color *in situ* hybridization at 36 hpf shows that *fsta* expression (red) is normal in *emx2* mutants, and *emx2* expression (red) is normal in *fsta* mutants. (E) Hyoid joint expression of *irx7* at 56 hpf is unaffected in *emx2* mutants and reduced in 2/7 *fsta; fstb* mutants. In green, *dlx2a* labels arch CNCCs and *sox9a* labels chondrocytes. Scale bars: 20 µm in C-E. (F) Model for Emx2 and Fsta function in the hyoid arch. At early stages, Fsta promotes *irx7* expression, preventing differentiation and cartilage matrix accumulation between Hm and Sy and allowing chondroprogenitors to rearrange into the single stack of Sy chondrocytes. Following rearrangements, Emx2 promotes chondrogenic differentiation to fuse Hm and Sy into a seamless cartilage. By contrast, there is a continuous requirement for Fsta function at the nearby hyoid joint to maintain its patency through active inhibition of chondrogenesis.

expression patterns and functions of genes not previously implicated in craniofacial development. The intersection of domain-specific gene expression with changes upon signaling perturbation uncovered distinct roles for Edn1 signaling along the dorsoventral axis that might help explain the complex phenotypes of *edn1* mutants. In particular, we identified new roles for two

Development (2017) 144, 2994-3005 doi:10.1242/dev.151712

distinctly regulated Edn1 target genes, *fsta* and *emx2*, in coordinating joint, cartilage, and bone morphogenesis in the intermediate regions of the developing arches.

Identification of novel domain-specific arch genes

We used two complementary methods to identify co-expressed modules of genes in mandibular and hyoid arch CNCCs. The first approach took advantage of the graded expression of *hand2*:GFP and *dlx5a*:GFP transgenes along the dorsoventral axis to group genes into four compartments, and the second approach mined co-variation across 19 RNAseq datasets to identify genes with similar expression patterns and/or regulation.

A limitation of the first strategy is that filtering thresholds are empirically determined, and that genes must pass all thresholds to be included (which is likely to account for some known genes, such as *dlx6a*, being excluded). Empirical shifting of thresholds, guided in part by anchoring well-characterized genes in each cluster, led to a balance between the number of false positives (genes not expressed in the predicted domains) and false negatives (genes with known domain-specific expression not being included). An advantage of the second, co-variance strategy is that it is unbiased, although both the relative enrichment in *hand2*:GFP^{+} and *dlx5a*:GFP^{+} domains and expression changes in response to signaling perturbation drive clustering. Nonetheless, considerable concordance between the approaches points to the validity of each. For example, four ventral genes (*pitx1*, *fzd9b*, *foxf1*, *foxf2a*), four ventral-intermediate genes (*dlx3b*, *dlx4b*, *dlx5a*, *msxe*) and five intermediate genes (*emx2*, *fsta*, *igfbp5b*, *grem2b*, *foxd1*) were similarly identified by *hand2*:GFP/*dlx5a*:GFP filtering and co-variance analysis.

Using these types of analyses, we uncovered a number of new genes with validated domain-specific expression. In the ventral domain, these included *S-phase kinase-associated protein 2* (*skp2*) and *mitochondrial ribosome recycling factor* (*mrrf*), perhaps reflecting distal growth of this domain to elongate the lower jaw (Bonilla-Claudio et al., 2012; Medeiros and Crump, 2012). In the ventral-intermediate domain we uncovered specific expression of Fgf-binding proteins (*fgfbp2a* and *fgfbp2b*), suggesting fine regulation of Fgf signaling in this domain. In the intermediate domain, we discovered two putative Bmp inhibitors (*fsta* and *ctgfb*) with tightly restricted expression near the developing hyoid joint, consistent with prior data showing that complex regulation of Bmp signaling is important for joint specification (Salazar et al., 2016; Smeeton et al., 2017). In the dorsal domain, we uncovered selective expression of genes previously implicated in earlier neural crest and ectomesenchyme development, including a Snail transcription factor (*snai1a*) (LaBonne and Bronner-Fraser, 2000), *cadherin 11* (*cdh11*) (McLennan et al., 2015), *potassium channel tetramerization domain-containing 15a* (*kctd15a*), which interacts with *tfap2a* (Zarelli and Dawid, 2013), and endosialin (*cd248a*) (Das and Crump, 2012); this signature is consistent with our previous findings that dorsal arch CNCCs differentiate later than other arch CNCCs (Barske et al., 2016). Of the 31 genes tested by *in situ* hybridization, 26 showed expression in the predicted domain, three showed CNCC-specific expression outside the predicted domain, and two were expressed in non-CNCC arch tissues. Further, applying WGCNA to the dorsoventral gene lists correctly predicted 4/5 false positives while only excluding 1/26 true positives. The one exception was *secreted frizzled-related protein 2* (*sfrp2*), which showed dorsal-specific expression in arch mesoderm but not CNCCs. Its mouse homolog has also been reported to be upregulated in *Dlx5/6* mutants, consistent with dorsal enrichment (Jeong et al., 2008). We do not know whether the inclusion of *sfrp2* in our CNCC datasets reflects expression in CNCCs below the level of detection by *in situ* hybridization or contamination of our FACS-sorted populations by a few non-CNCC arch cells. Nonetheless, our analysis pipeline accurately predicted domain-specific expression for a high proportion of genes, including nine not previously implicated in craniofacial development.

Region-specific roles of Edn1 and Jagged-Notch signaling in arch patterning

Previous work had suggested greater roles for Edn1 signaling in intermediate versus more ventral domains (Alexander et al., 2011; Zuniga et al., 2011), and for Jagged-Notch signaling in the dorsal arches (Zuniga et al., 2010). By analyzing how gene modules of distinct arch domains are affected by signaling perturbations, we confirm this on a genomic scale (as summarized in Fig. 4E). A more prominent role for Edn1 in controlling gene expression in intermediate mandibular and hyoid arch domains, which generate joints and the palatoquadrate and symplectic cartilages, helps explain why these skeletal elements are most sensitive to partial reduction of Edn1 function (Miller and Kimmel, 2001) and mutation of its downstream effectors Plcb3 and Mef2ca (Walker et al., 2006, 2007). Conversely, the ventralmost elements of the mandibular and hyoid arches, such as the basihyal, are spared in severe *edn1* mutants (Miller et al., 2000), consistent with the expression of most ventral genes in this study (*smad6a*, *skp2*, *fzd9b*) and in previous reports (*satb2*) (Sheehan-Rooney et al., 2013a) being unaffected by Edn1 perturbations. However, some ventral genes, such as *hand2* and *pitx1*, are lost in *edn1* mutants, although regulation of *hand2* may be indirect through the Edn1 targets Dlx5/6 (Miller et al., 2003; Yanagisawa et al., 2003). Edn1-independent ventral genes might instead depend on Bmp signaling. *Smad6* and *Satb2* were identified as direct targets of Bmp-dependent pSmads in mice (Bonilla-Claudio et al., 2012), and *satb2* is a target of Bmp signaling in zebrafish (Sheehan-Rooney et al., 2013a).

In the dorsal domain, only a subset of genes are regulated by Jagged-Notch signaling (e.g. *cd248a*, *pou3f3a* and *pou3f3b*, but not *cdh11* and *kctd15a*), consistent with the relatively mild dorsal phenotypes of *jag1b* and *notch2; notch3* mutants (Zuniga et al., 2010; Barske et al., 2016) and suggesting Notch-independent regulation of some aspects of dorsal identity.

Whereas we found generally good correspondence between changes in RNAseq values and *in situ* validation in *edn1* and *jag1b* mutants, *in situ* validation but not RNAseq revealed differences in *stmn1a*, *sema3bl* and *cdh11* expression in *edn1* mutants. As *stmn1a* and *sema3bl* show broad arch expression, profiling all arch CNCCs is likely to dilute the effect of selective loss of their ventral expression domains in mutants. Likewise, a shift of *cdh11* expression from dorsal to ventral domains in mutants would not necessarily result in a total expression difference throughout arch CNCCs. These findings suggest that examining expression changes in CNCCs sorted from distinct arch domains in animals with signaling perturbations might be a better way to detect how signaling affects expression patterns.

A lack of obvious craniofacial phenotypes in mutants for many arch-specific genes

The ease of genetic manipulation makes zebrafish an attractive system for performing reverse genetic analysis of craniofacial development. However, homozygous loss-of-function mutants for only two of the 12 domain-specific genes tested showed clear facial cartilage and/or bone phenotypes in larvae. There are several

Development (2017) 144, 2994-3005 doi:10.1242/dev.151712

possible explanations for the lack of observable phenotypes. First, although we selected mutations causing premature translational termination before crucial conserved domains, it remains possible that some mutations do not create true nulls. Second, some mutants might have craniofacial defects that we failed to appreciate, for example in other arch derivatives such as ligaments or long-lived progenitors. Third, maternal contribution of mRNA and/or protein could compensate for zygotic loss-of-function. In some cases (e.g. *ctgfa*), maternal-zygotic null mutants did not display larval craniofacial defects. The growth delay and tail fin regeneration defects of *mrrf* mutants could be explained by depletion of remaining maternal stores, similar to previous reports for other mutants in mitochondrial proteins (Rahn et al., 2015). It thus remains possible that *mrrf* expression in the ventralmost arches reflects rapid growth and/or metabolism of this domain. Fourth, there might be genetic compensation (Rossi et al., 2015). Large-scale mutational screens in zebrafish have found a surprisingly small number of genes required for larval viability (~6%), suggesting a high degree of genetic redundancy in zebrafish (Kettleborough et al., 2013). In addition, the identification of multiple alleles for craniofacial mutants suggests that previous screens are approaching saturation for obvious larval skeletal defects (Neuhauss et al., 1996; Piotrowski et al., 1996; Schilling et al., 1996; Nissen et al., 2006). Our findings therefore indicate that many of the single gene mutants with obvious craniofacial patterning defects in zebrafish might have already been found.

Complex regulation by Edn1 coordinates intermediate arch morphogenesis

A curious feature of *edn1* mutants, as well as mutants for its effector *mef2ca*, is the phenotypic variability of intermediate domain-derived skeletal elements, including joints and the opercle bone (Kimmel et al., 2003; DeLaurier et al., 2014). Our analysis of two newly identified Edn1 target genes, *emx2* and *fsta*, may shed some light on this variability. For example, the gain or loss of the opercle in *edn1* mutants might reflect the observed variability in *emx2* regulation, given that loss of *emx2* suppressed the opercle expansion seen in some *edn1* mutants without rescuing ventral cartilage loss (Fig. S4). The loss of the hyoid joint and the reduction in symplectic cartilage in *fsta* mutants are also similar to what is seen in hypomorphic Edn1 pathway mutants (Miller et al., 2000; Walker et al., 2006, 2007; DeLaurier et al., 2014), consistent with our finding that intermediate domain *fsta* expression is lost in *edn1* mutants. Our previous analysis of similar phenotypes in *irx7; irx5a* compound mutants showed that inappropriate chondrogenic differentiation at the junction between the nascent symplectic and hyomandibular cartilages prevents these cells from rearranging and thus lengthening the symplectic (Askary et al., 2015). By contrast, the hyomandibular and symplectic cartilages fail to connect in *emx2* mutants. Temporal regulation by Edn1 in the intermediate domain may therefore result in Fsta blocking cartilage differentiation at early stages to allow symplectic elongation, with Emx2 promoting cartilage differentiation at later stages to fuse the symplectic and hyomandibular into a seamless cartilage (Fig. 6F). As Bmp activity inhibits *irx7* expression (Askary et al., 2015), Fsta might promote *irx7* at the hyoid joint by limiting Bmp signaling. The low penetrance of *irx7* loss and joint fusion in *fsta/b* mutants might be due to functional redundancy with other putative Bmp inhibitors expressed at the joint, including *ctgfb* (this study), *grem2b* (Zuniga et al., 2011) and *chordin* (Miller et al., 2003). Interestingly, *Emx2* mutant mice lack the incus cartilage of the middle ear (Rhodes et al., 2003), which is homologous to the palatoquadrate affected in fish *emx2* mutants. Part of the arch patterning function of Emx2 might thus be conserved from fish to mammals.

Our transcriptome-driven analysis of arch regionalization has therefore provided new insights into how Edn1 signaling regulates a delicate balance of cartilage differentiation to fine-tune skeletal shape. In the future, the analysis pipeline presented here should help to reveal regulatory changes in additional mutants that disrupt facial patterning.

MATERIALS AND METHODS

Zebrafish lines

The University of Southern California Institutional Animal Care and Use Committee approved all experiments on zebrafish (*Danio rerio*). Published lines include *Tg(hand2:eGFP)* (Kikuchi et al., 2011), *dlx5a*^{i1073Et} (referred to here as *dlx5a:GFP*) (Talbot et al., 2010), *Tg(fli1a:eGFP)*^{y1} (Lawson and Weinstein, 2002), *Tg(sox10:DsRed-Express)*^{el10} (Das and Crump, 2012), *Tg(sox10:GFPCAAX)*, *irx7*^{el538}, *irx5*^{el574} (Askary et al., 2015), *sucker/edn1*^{tf216} (Miller et al., 2000) and *jag1b*^{b1105} (Zuniga et al., 2010).

FACS and RNAseq

fli1a:GFP; sox10:DsRed and *hand2:GFP; sox10:DsRed* fish were incrossed to generate embryos, and *dlx5a:GFP; sox10:DsRed* fish were outcrossed to avoid homozygosity of the *dlx5a*^{i1073Et} insertional allele. Embryos were dissociated as previously described (Covassin et al., 2006), with minor modifications (Barske et al., 2016). Cells were sorted based on GFP and DsRed expression on a MoFlo Astrios instrument (Beckman-Coulter) into RLT lysis buffer (Qiagen), and total RNA was extracted using the RNeasy Micro Kit (Qiagen). RNA integrity was assessed on Bioanalyzer Pico RNA chips (Agilent), cDNA synthesized with the SMART-Seq Ultra Low Input RNA Kit (Clontech), and libraries generated with the Kapa Hyper Prep Kit (Kapa Biosystems) and NextFlex adapters (Bioo Scientific). 75 bp paired-end sequencing was performed on a NextSeq 500 machine (Illumina).

RNAseq data analysis and statistical tests

After trimming using Partek Flow default criteria, sequencing reads were aligned to zebrafish GRCz10 (Ensembl_v80) using TopHat 2 (https://ccb.jhu.edu/software/tophat/index.shtml). Aligned reads were quantified using Partek E/M and normalized to yield TPM values, controlling for sequencing depth disparities across samples (Wagner et al., 2012). Data are accessible through GEO series accession GSE95812. To test whether $\log_2$ fold-change values for each group of genes were significantly different to zero (Fig. 3), we used the Shapiro-Wilk test for normality to determine whether a one-sample *t*-test or a Wilcoxon signed-rank test was appropriate. The Bonferroni correction was then applied on the resulting *P*-values of one-tailed tests to account for multiple comparisons. The Mann–Whitney *U*-test for two independent samples was performed in Excel 2016 (Microsoft) using Real Statistics Resource Pack software (release 4.9; www.real-statistics.com) to compare effects of Edn1 and Notch signaling, as the data from at least one group were not distributed normally.

Co-variance analysis

A weighted gene co-expression network analysis (WGCNA) (Langfelder and Horvath, 2008) was run on *m* genes exhibiting the highest variance across *n* samples (m=6000, n=19), yielding an $m \times m$ topological overlap matrix (TOM) that links genes by correspondence of correlated genes. The exponent β was selected to yield scale-free topology as defined by minimum power required to output maximal R^2. We computed the TOM driver array (TDA) by taking the average TOM value across genes of interest, then deriving the deviation in TOM when each sample was removed:

$$TDA_i = \frac{mean(TOM) - mean(TOM_i)}{mean(TOM)}. \quad (1)$$

Development (2017) 144, 2994-3005 doi:10.1242/dev.151712

These values are normalized to produce nTDA, which spans [−1,1]:

$$nTDA_i = if\ (TDA_i \geq 0)\ \frac{TDA_i}{\max\{\ TDA_1, TDA_2, \ldots, TDA_n\}} = if\ (TDA_1 < 0)\frac{TDA_i}{\min\{TDA_1, TDA_2, \ldots, TDA_n\}}. \quad (2)$$

Samples with a positive TDA drive clustering, whereas samples with negative TDA disrupt clustering.

In situ hybridization and immunohistochemistry

Partial cDNAs were PCR amplified with Herculase II Fusion Polymerase (Agilent), cloned into pCR_Blunt_II_Topo (ThermoFisher Scientific), linearized, and synthesized with SP6 or T7 RNA polymerase (Roche Life Sciences) as specified (Table S3). *In situ* hybridization was performed as described (Zuniga et al., 2010), co-staining for *dlx2a* (Akimenko et al., 1994), *sox9a*, or with rabbit anti-GFP antibody (Torrey Pines Biolabs, TP401; 1:1000) to highlight arch CNCCs or early cartilages. Imaging was performed with a Zeiss LSM800 confocal microscope and presented as optical sections or maximum intensity projections as specified. Typically, six to ten controls and three to seven mutants were imaged for each probe.

Mutant generation and skeletal staining

Twelve mutant lines were created via TALEN (Sanjana et al., 2012) or CRISPR/Cas9 (Jao et al., 2013) mutagenesis as described (Barske et al., 2016). Germline founders were detected by screening their F1 progeny by restriction digestion of PCR products, followed by sequencing to identify frameshift indels (Table S2). Alcian Blue and Alizarin Red staining of cartilage and bone were performed as described (Walker and Kimmel, 2007). Symplectic cartilage length was measured with ImageJ (NIH) and compared using unpaired *t*-tests.

Acknowledgements

We thank Megan Matsutani and Jennifer DeKoeyer Crump for fish care, Lora Barsky and Jeffrey Boyd at the USC Stem Cell Flow Cytometry Core Facility for FACS, Charles Nicolet at the USC Norris Cancer Center Molecular Genomics Core for sequencing, and Yibu Chen for sequencing analysis.

Competing interests

The authors declare no competing or financial interests.

Author contributions

Conceptualization: A.A., P.X., L.B., B.B., J.G.C.; Methodology: A.A., P.X., L.B., P.B., B.B.; Software: A.A., M.B.; Validation: A.A., L.B.; Formal analysis: A.A., P.X., L.B., J.G.C.; Investigation: A.A., P.X., L.B., P.B.; Resources: A.A., J.G.C.; Data curation: A.A., P.X., L.B., M.B.; Writing - original draft: A.A., P.X., L.B., M.B., J.G.C.; Writing - review & editing: A.A., P.X., L.B., M.A.B., J.G.C.; Supervision: M.A.B., J.G.C.; Project administration: J.G.C.; Funding acquisition: M.A.B., J.G.C.

Funding

Research was funded by grants from the National Institute of Dental and Craniofacial Research (NIDCR) (DE018405) to J.G.C., National Institute of Neurological Disorders and Stroke (R00NS080913) to M.A.B., A.P. Giannini Foundation and NIDCR (K99DE026239) to L.B., and National Institute on Deafness and Other Communication Disorders (training grant T32 DC009975) to A.A. Deposited in PMC for release after 12 months.

Data availability

RNAseq data are available at Gene Expression Omnibus through series accession number GSE95812.

Supplementary information

Supplementary information available online at
http://dev.biologists.org/lookup/doi/10.1242/dev.151712.supplemental

References

Akimenko, M. A., Ekker, M., Wegner, J., Lin, W. and Westerfield, M. (1994). Combinatorial expression of three zebrafish genes related to distal-less: part of a homeobox gene code for the head. *J. Neurosci.* **14**, 3475-3486.

Alexander, C., Zuniga, E., Blitz, I. L., Wada, N., Le Pabic, P., Javidan, Y., Zhang, T., Cho, K. W., Crump, J. G. and Schilling, T. F. (2011). Combinatorial roles for BMPs and Endothelin 1 in patterning the dorsal-ventral axis of the craniofacial skeleton. *Development* **138**, 5135-5146.

Askary, A., Mork, L., Paul, S., He, X., Izuhara, A. K., Gopalakrishnan, S., Ichida, J. K., McMahon, A. P., Dabizljevic, S., Dale, R. et al. (2015). Iroquois proteins promote skeletal joint formation by maintaining chondrocytes in an immature state. *Dev. Cell* **35**, 358-365.

Barske, L., Askary, A., Zuniga, E., Balczerski, B., Bump, P., Nichols, J. T. and Crump, J. G. (2016). Competition between Jagged-Notch and endothelin1 signaling selectively restricts cartilage formation in the zebrafish upper face. *PLoS Genet.* **12**, e1005967.

Beverdam, A., Merlo, G. R., Paleari, L., Mantero, S., Genova, F., Barbieri, O., Janvier, P. and Levi, G. (2002). Jaw transformation with gain of symmetry after Dlx5/Dlx6 inactivation: mirror of the past? *Genesis* **34**, 221-227.

Bonilla-Claudio, M., Wang, J., Bai, Y., Klysik, E., Selever, J. and Martin, J. F. (2012). Bmp signaling regulates a dose-dependent transcriptional program to control facial skeletal development. *Development* **139**, 709-719.

Bronner, M. E. and LeDouarin, N. M. (2012). Development and evolution of the neural crest: an overview. *Dev. Biol.* **366**, 2-9.

Brunskill, E. W., Potter, A. S., Distasio, A., Dexheimer, P., Plassard, A., Aronow, B. J. and Potter, S. S. (2014). A gene expression atlas of early craniofacial development. *Dev. Biol.* **391**, 133-146.

Clouthier, D. E., Hosoda, K., Richardson, J. A., Williams, S. C., Yanagisawa, H., Kuwaki, T., Kumada, M., Hammer, R. E. and Yanagisawa, M. (1998). Cranial and cardiac neural crest defects in endothelin-A receptor-deficient mice. *Development* **125**, 813-824.

Compagnucci, C., Debiais-Thibaud, M., Coolen, M., Fish, J., Griffin, J. N., Bertocchini, F., Minoux, M., Rijli, F. M., Borday-Birraux, V., Casane, D. et al. (2013). Pattern and polarity in the development and evolution of the gnathostome jaw: both conservation and heterotopy in the branchial arches of the shark, Scyliorhinus canicula. *Dev. Biol.* **377**, 428-448.

Covassin, L., Amigo, J. D., Suzuki, K., Teplyuk, V., Straubhaar, J. and Lawson, N. D. (2006). Global analysis of hematopoietic and vascular endothelial gene expression by tissue specific microarray profiling in zebrafish. *Dev. Biol.* **299**, 551-562.

Das, A. and Crump, J. G. (2012). Bmps and id2a act upstream of Twist1 to restrict ectomesenchyme potential of the cranial neural crest. *PLoS Genet.* **8**, e1002710.

DeLaurier, A., Huycke, T. R., Nichols, J. T., Swartz, M. E., Larsen, A., Walker, C., Dowd, J., Pan, L., Moens, C. B. and Kimmel, C. B. (2014). Role of mef2ca in developmental buffering of the zebrafish larval hyoid dermal skeleton. *Dev. Biol.* **385**, 189-199.

Depew, M. J., Lufkin, T. and Rubenstein, J. L. (2002). Specification of jaw subdivisions by Dlx genes. *Science* **298**, 381-385.

Feng, J., Bi, C., Clark, B. S., Mady, R., Shah, P. and Kohtz, J. D. (2006). The Evf-2 noncoding RNA is transcribed from the Dlx-5/6 ultraconserved region and functions as a Dlx-2 transcriptional coactivator. *Genes Dev.* **20**, 1470-1484.

Feng, W., Leach, S. M., Tipney, H., Phang, T., Geraci, M., Spritz, R. A., Hunter, L. E. and Williams, T. (2009). Spatial and temporal analysis of gene expression during growth and fusion of the mouse facial prominences. *PLoS ONE* **4**, e8066.

Fujita, K., Taya, Y., Shimazu, Y., Aoba, T. and Soeno, Y. (2013). Molecular signaling at the fusion stage of the mouse mandibular arch: involvement of insulin-like growth factor family. *Int. J. Dev. Biol.* **57**, 399-406.

Germanguz, I., Lev, D., Waisman, T., Kim, C. H. and Gitelman, I. (2007). Four twist genes in zebrafish, four expression patterns. *Dev. Dyn.* **236**, 2615-2626.

Gharbi, N., Zhao, X.-F., Ellingsen, S. and Fjose, A. (2012). Zebrafish enhancer trap line showing maternal and neural expression of kctd15a. *Dev. Growth Differ.* **54**, 241-252.

Gordon, C. T., Petit, F., Kroisel, P. M., Jakobsen, L., Zechi-Ceide, R. M., Oufadem, M., Bole-Feysot, C., Pruvost, S., Masson, C., Tores, F. et al. (2013). Mutations in endothelin 1 cause recessive auriculocondylar syndrome and dominant isolated question-mark ears. *Am. J. Hum. Genet.* **93**, 1118-1125.

Hooper, J. E., Feng, W., Li, H., Leach, S. M., Phang, T., Siska, C., Jones, K. L., Spritz, R. A., Hunter, L. E. and Williams, T. (2017). Systems biology of facial development: contributions of ectoderm and mesenchyme. *Dev. Biol.* **426**, 97-114.

Hunter, M. P. and Prince, V. E. (2002). Zebrafish hox paralogue group 2 genes function redundantly as selector genes to pattern the second pharyngeal arch. *Dev. Biol.* **247**, 367-389.

Jao, L.-E., Wente, S. R. and Chen, W. (2013). Efficient multiplex biallelic zebrafish genome editing using a CRISPR nuclease system. *Proc. Natl. Acad. Sci. USA* **110**, 13904-13909.

Jeong, J., Mao, J., Tenzen, T., Kottmann, A. H. and McMahon, A. P. (2004). Hedgehog signaling in the neural crest cells regulates the patterning and growth of facial primordia. *Genes Dev.* **18**, 937-951.

Jeong, J., Li, X., McEvilly, R. J., Rosenfeld, M. G., Lufkin, T. and Rubenstein, J. L. R. (2008). Dlx genes pattern mammalian jaw primordium by regulating both lower jaw-specific and upper jaw-specific genetic programs. *Development* **135**, 2905-2916.

Development (2017) 144, 2994-3005 doi:10.1242/dev.151712

Kettleborough, R. N. W., Busch-Nentwich, E. M., Harvey, S. A., Dooley, C. M., de Bruijn, E., van Eeden, F., Sealy, I., White, R. J., Herd, C., Nijman, I. J. et al. (2013). A systematic genome-wide analysis of zebrafish protein-coding gene function. *Nature* **496**, 494-497.

Kikuchi, K., Holdway, J. E., Major, R. J., Blum, N., Dahn, R. D., Begemann, G. and Poss, K. D. (2011). Retinoic acid production by endocardium and epicardium is an injury response essential for zebrafish heart regeneration. *Dev. Cell* **20**, 397-404.

Kimmel, C. B., Miller, C. T., Kruze, G., Ullmann, B., BreMiller, R. A., Larison, K. D. and Snyder, H. C. (1998). The shaping of pharyngeal cartilages during early development of the zebrafish. *Dev. Biol.* **203**, 245-263.

Kimmel, C. B., Ullmann, B., Walker, M., Miller, C. T. and Crump, J. G. (2003). Endothelin 1-mediated regulation of pharyngeal bone development in zebrafish. *Development* **130**, 1339-1351.

Kurihara, Y., Kurihara, H., Suzuki, H., Kodama, T., Maemura, K., Nagai, R., Oda, H., Kuwaki, T., Cao, W.-H., Kamada, N. et al. (1994). Elevated blood pressure and craniofacial abnormalities in mice deficient in endothelin-1. *Nature* **368**, 703-710.

LaBonne, C. and Bronner-Fraser, M. (2000). Snail-related transcriptional repressors are required in Xenopus for both the induction of the neural crest and its subsequent migration. *Dev. Biol.* **221**, 195-205.

Langfelder, P. and Horvath, S. (2008). WGCNA: an R package for weighted correlation network analysis. *BMC Bioinformatics* **9**, 559.

Lawson, N. D. and Weinstein, B. M. (2002). In vivo imaging of embryonic vascular development using transgenic zebrafish. *Dev. Biol.* **248**, 307-318.

McLennan, R., Schumacher, L. J., Morrison, J. A., Teddy, J. M., Ridenour, D. A., Box, A. C., Semerad, C. L., Li, H., McDowell, W., Kay, D. et al. (2015). Neural crest migration is driven by a few trailblazer cells with a unique molecular signature narrowly confined to the invasive front. *Development* **142**, 2014-2025.

Medeiros, D. M. and Crump, J. G. (2012). New perspectives on pharyngeal dorsoventral patterning in development and evolution of the vertebrate jaw. *Dev. Biol.* **371**, 121-135.

Miller, C. T. and Kimmel, C. B. (2001). Morpholino phenocopies of endothelin 1 (sucker) and other anterior arch class mutations. *Genesis* **30**, 186-187.

Miller, C. T., Schilling, T. F., Lee, K., Parker, J. and Kimmel, C. B. (2000). sucker encodes a zebrafish Endothelin-1 required for ventral pharyngeal arch development. *Development* **127**, 3815-3828.

Miller, C. T., Yelon, D., Stainier, D. Y. R. and Kimmel, C. B. (2003). Two endothelin 1 effectors, hand2 and bapx1, pattern ventral pharyngeal cartilage and the jaw joint. *Development* **130**, 1353-1365.

Minoux, M. and Rijli, F. M. (2010). Molecular mechanisms of cranial neural crest cell migration and patterning in craniofacial development. *Development* **137**, 2605-2621.

Mork, L. and Crump, G. (2015). Zebrafish craniofacial development: a window into early patterning. *Curr. Top. Dev. Biol.* **115**, 235-269.

Nair, S., Li, W., Cornell, R. and Schilling, T. F. (2007). Requirements for Endothelin type-A receptors and Endothelin-1 signaling in the facial ectoderm for the patterning of skeletogenic neural crest cells in zebrafish. *Development* **134**, 335-345.

Neuhauss, S. C., Solnica-Krezel, L., Schier, A. F., Zwartkruis, F., Stemple, D. L., Malicki, J., Abdelilah, S., Stainier, D. Y. and Driever, W. (1996). Mutations affecting craniofacial development in zebrafish. *Development* **123**, 357-367.

Nichols, J. T., Pan, L., Moens, C. B. and Kimmel, C. B. (2013). barx1 represses joints and promotes cartilage in the craniofacial skeleton. *Development* **140**, 2765-2775.

Nichols, J. T., Blanco-Sánchez, B., Brooks, E. P., Parthasarathy, R., Dowd, J., Subramanian, A., Nachtrab, G., Poss, K. D., Schilling, T. F. and Kimmel, C. B. (2016). Ligament versus bone cell identity in the zebrafish hyoid skeleton is regulated by mef2ca. *Development* **143**, 4430-4440.

Nissen, R. M., Amsterdam, A. and Hopkins, N. (2006). A zebrafish screen for craniofacial mutants identifies wdr68 as a highly conserved gene required for endothelin-1 expression. *BMC Dev. Biol.* **6**, 28.

Ozeki, H., Kurihara, Y., Tonami, K., Watatani, S. and Kurihara, H. (2004). Endothelin-1 regulates the dorsoventral branchial arch patterning in mice. *Mech. Dev.* **121**, 387-395.

Paul, S., Schindler, S., Giovannone, D., de Millo Terrazzani, A., Mariani, F. V. and Crump, J. G. (2016). Ihha induces hybrid cartilage-bone cells during zebrafish jawbone regeneration. *Development* **143**, 2066-2076.

Piotrowski, T., Schilling, T. F., Brand, M., Jiang, Y. J., Heisenberg, C. P., Beuchle, D., Grandel, H., van Eeden, F. J., Furutani-Seiki, M., Granato, M. et al. (1996). Jaw and branchial arch mutants in zebrafish II: anterior arches and cartilage differentiation. *Development* **123**, 345-356.

Platt, J. B. (1893). Ectodermic origin of the cartilages of the head. *Anat. Anz.* **8**, 506-509.

Rahn, J. J., Bestman, J. E., Stackley, K. D. and Chan, S. S. L. (2015). Zebrafish lacking functional DNA polymerase gamma survive to juvenile stage, despite rapid and sustained mitochondrial DNA depletion, altered energetics and growth. *Nucleic Acids Res.* **43**, 10338-10352.

Rhodes, C. R., Parkinson, N., Tsai, H., Brooker, D., Mansell, S., Spurr, N., Hunter, A. J., Steel, K. P. and Brown, S. D. M. (2003). The homeobox gene Emx2 underlies middle ear and inner ear defects in the deaf mouse mutant pardon. *J. Neurocytol.* **32**, 1143-1154.

Rossi, A., Kontarakis, Z., Gerri, C., Nolte, H., Hölper, S., Krüger, M. and Stainier, D. Y. R. (2015). Genetic compensation induced by deleterious mutations but not gene knockdowns. *Nature* **524**, 230-233.

Salazar, V. S., Gamer, L. W. and Rosen, V. (2016). BMP signalling in skeletal development, disease and repair. *Nat. Rev. Endocrinol.* **12**, 203-221.

Sanjana, N. E., Cong, L., Zhou, Y., Cunniff, M. M., Feng, G. and Zhang, F. (2012). A transcription activator-like effector toolbox for genome engineering. *Nat. Protoc.* **7**, 171-192.

Sato, T., Kurihara, Y., Asai, R., Kawamura, Y., Tonami, K., Uchijima, Y., Heude, E., Ekker, M., Levi, G. and Kurihara, H. (2008). An endothelin-1 switch specifies maxillomandibular identity. *Proc. Natl. Acad. Sci. USA* **105**, 18806-18811.

Schilling, T. F. and Kimmel, C. B. (1994). Segment and cell type lineage restrictions during pharyngeal arch development in the zebrafish embryo. *Development* **120**, 483-494.

Schilling, T. F., Piotrowski, T., Grandel, H., Brand, M., Heisenberg, C. P., Jiang, Y. J., Beuchle, D., Hammerschmidt, M., Kane, D. A., Mullins, M. C. et al. (1996). Jaw and branchial arch mutants in zebrafish I: branchial arches. *Development* **123**, 329-344.

Sheehan-Rooney, K., Swartz, M. E., Lovely, C. B., Dixon, M. J. and Eberhart, J. K. (2013a). Bmp and Shh signaling mediate the expression of satb2 in the pharyngeal arches. *PLoS ONE* **8**, e59533.

Sheehan-Rooney, K., Swartz, M. E., Zhao, F., Liu, D. and Eberhart, J. K. (2013b). Ahsa1 and Hsp90 activity confers more severe craniofacial phenotypes in a zebrafish model of hypoparathyroidism, sensorineural deafness and renal dysplasia (HDR). *Dis. Model. Mech.* **6**, 1285-1291.

Smeeton, J., Askary, A. and Crump, J. G. (2017). Building and maintaining joints by exquisite local control of cell fate. *Wiley Interdiscip. Rev. Dev. Biol.* **6**, doi: 10.1002/wdev.245.

Sperber, S. M., Saxena, V., Hatch, G. and Ekker, M. (2008). Zebrafish dlx2a contributes to hindbrain neural crest survival, is necessary for differentiation of sensory ganglia and functions with dlx1a in maturation of the arch cartilage elements. *Dev. Biol.* **314**, 59-70.

Swartz, M. E., Sheehan-Rooney, K., Dixon, M. J. and Eberhart, J. K. (2011). Examination of a palatogenic gene program in zebrafish. *Dev. Dyn.* **240**, 2204-2220.

Talbot, J. C., Johnson, S. L. and Kimmel, C. B. (2010). hand2 and Dlx genes specify dorsal, intermediate and ventral domains within zebrafish pharyngeal arches. *Development* **137**, 2507-2517.

Thomas, T., Kurihara, H., Yamagishi, H., Kurihara, Y., Yazaki, Y., Olson, E. N. and Srivastava, D. (1998). A signaling cascade involving endothelin-1, dHAND and msx1 regulates development of neural-crest-derived branchial arch mesenchyme. *Development* **125**, 3005-3014.

Tucker, A. S., Matthews, K. L. and Sharpe, P. T. (1998). Transformation of tooth type induced by inhibition of BMP signaling. *Science* **282**, 1136-1138.

Wagner, G. P., Kin, K. and Lynch, V. J. (2012). Measurement of mRNA abundance using RNA-seq data: RPKM measure is inconsistent among samples. *Theory Biosci.* **131**, 281-285.

Walker, M. B. and Kimmel, C. B. (2007). A two-color acid-free cartilage and bone stain for zebrafish larvae. *Biotech. Histochem.* **82**, 23-28.

Walker, M. B., Miller, C. T., Coffin Talbot, J., Stock, D. W. and Kimmel, C. B. (2006). Zebrafish furin mutants reveal intricacies in regulating Endothelin1 signaling in craniofacial patterning. *Dev. Biol.* **295**, 194-205.

Walker, M. B., Miller, C. T., Swartz, M. E., Eberhart, J. K. and Kimmel, C. B. (2007). phospholipase C, beta 3 is required for Endothelin1 regulation of pharyngeal arch patterning in zebrafish. *Dev. Biol.* **304**, 194-207.

Yanagisawa, H., Clouthier, D. E., Richardson, J. A., Charite, J. and Olson, E. N. (2003). Targeted deletion of a branchial arch-specific enhancer reveals a role of dHAND in craniofacial development. *Development* **130**, 1069-1078.

Zarelli, V. E. and Dawid, I. B. (2013). Inhibition of neural crest formation by Kctd15 involves regulation of transcription factor AP-2. *Proc. Natl. Acad. Sci. USA* **110**, 2870-2875.

Zhang, B. and Horvath, S. (2005). A general framework for weighted gene co-expression network analysis. *Stat. Appl. Genet. Mol. Biol.* **4**, Article17.

Zuniga, E., Stellabotte, F. and Crump, J. G. (2010). Jagged-Notch signaling ensures dorsal skeletal identity in the vertebrate face. *Development* **137**, 1843-1852.

Zuniga, E., Rippen, M., Alexander, C., Schilling, T. F. and Crump, J. G. (2011). Gremlin 2 regulates distinct roles of BMP and Endothelin 1 signaling in dorsoventral patterning of the facial skeleton. *Development* **138**, 5147-5156.

Supplementary Information

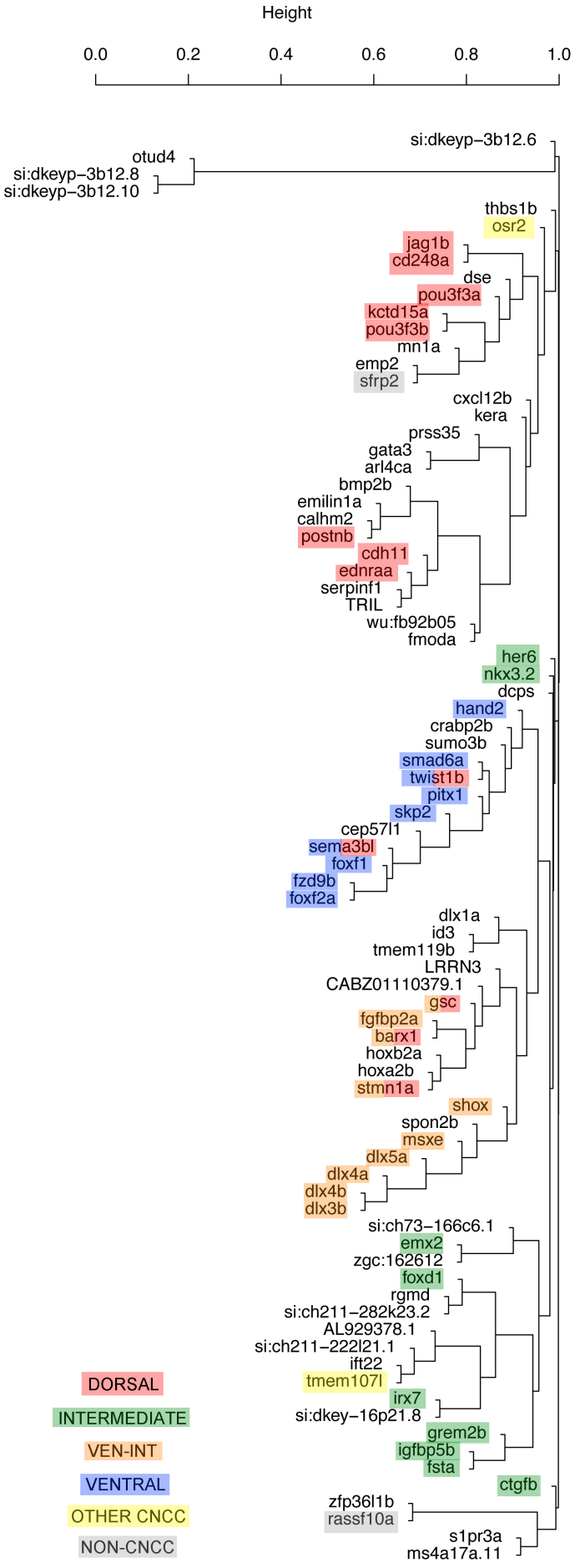

Supplementary Figure 1. WGCNA analysis of the dorsoventral gene list.

WGCNA analysis (see also Figure 5 and Methods) was applied to the more restricted dorsoventral gene list from Table 1 to reveal clusters of co-varying genes, which are color-coded based on known and/or validated in situ expression in the zebrafish pharyngeal arches at 36 hpf. Two-color shading denotes expression in both domains. Height refers to TOM dissimilarity – 0 indicates perfect co-variation between genes and 1 indicates complete lack of co-variation. This analysis confirms in situ validation showing that *rassf10a* and *osr2* were incorrectly assigned to the dorsal list, and *tmem107l* and *her6* incorrectly assigned to the ventral-intermediate (ven-int) list.

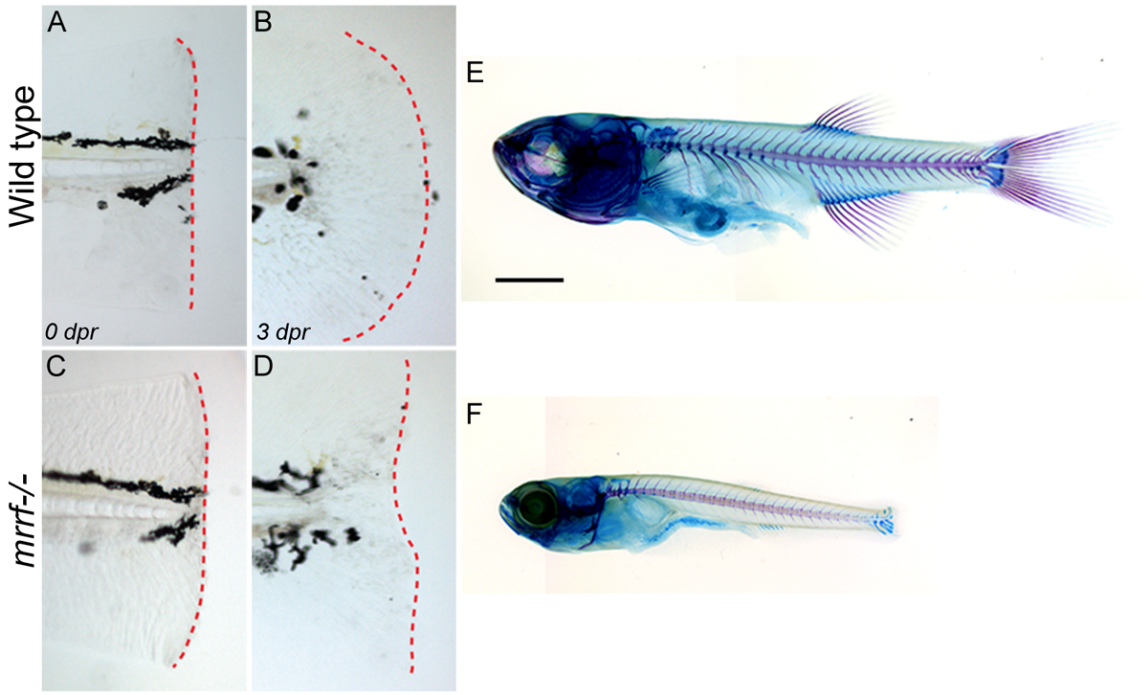

Supplementary Figure 2. Growth delay and defective fin regeneration in *mrrf* mutants.

(A-D) Wild-type and *mrrf*-/- embryos had their tail fins amputated at 3 dpf. The dotted red lines show the caudal extent of the tail fin and the lack of regeneration in mutants 3 days post-resection (dpr). (E and F) Alcian blue and Alizarin red staining of cartilage and bone, respectively, show a severe growth defect in *mrrf* mutants at one month of age. Scale bar = 100 μm.

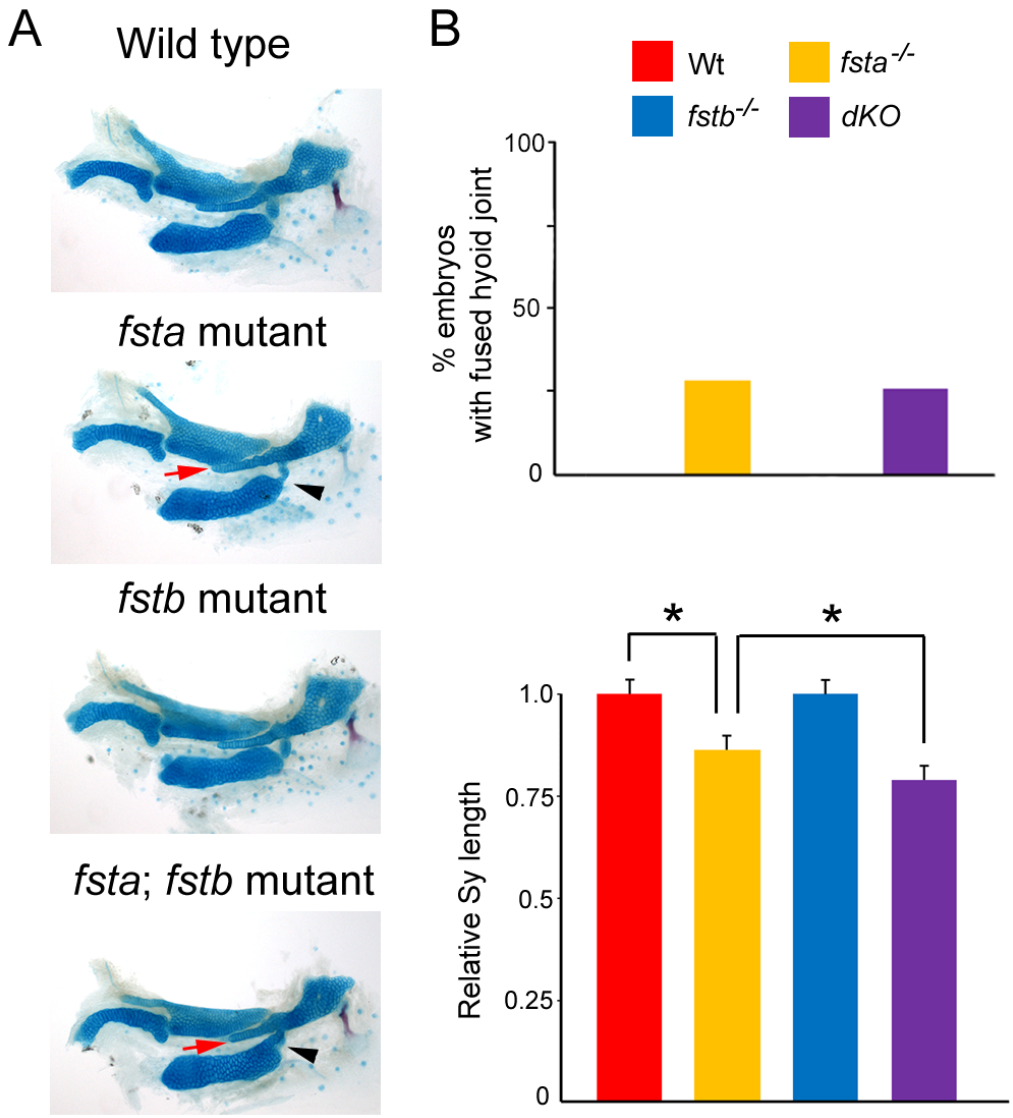

Supplementary Figure 3. Redundancy of *fsta* and *fstb* in hyoid skeletal development. (A) Alcian blue and Alizarin red staining of control, *fsta*, *fstb*, and *fsta*; *fstb* double mutant embryos at 5 dpf. In *fsta* but not *fstb* single mutants, the Sy is shortened (red arrow), and the hyoid joint is fused (black arrowhead). *fsta*; *fstb* double mutants display a slight enhancement of craniofacial defects compared to *fsta* mutants. (B) Quantification of fused hyoid joints and Sy length (number of sides examined for *fsta*, *fstb*, and *fsta; fstb* mutants = 14, 10 and 23, respectively). *$p < 0.05$ in student's *t*-test.

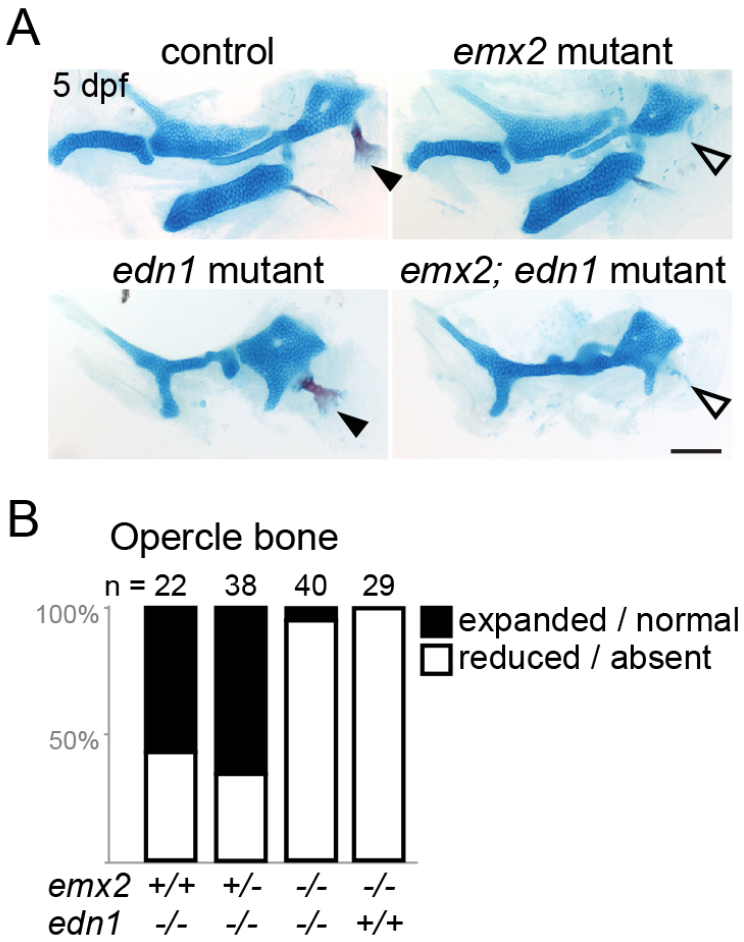

Supplementary Figure 4. Analysis of *emx2*; *edn1* compound mutants.

(A) Alcian blue and Alizarin red staining of control, *emx2*, *edn1*, and *emx2*; *edn1* double mutant embryos at 5 dpf. In *edn1* mutants, the opercle bone is variably expanded / normal (closed arrowhead) or reduced / absent (open arrowhead). In *emx2* and *emx2*; *edn1* mutants, the opercle is almost always reduced or absent. In addition, loss of *emx2* fails to rescue the reduced ventral cartilage in *edn1* mutants. Scale bar = 100 μm.

(B) Quantification of the percentage of opercle bone defects in single and double mutants. The number of sides examined is listed above each bar. The decrease in the proportion of larvae with expanded / normal opercle bone in $emx2^{-/-}$; $edn1^{-/-}$ mutants compared with $emx2^{+/+}$; $edn1^{-/-}$ was significant at $p < 0.0001$ (two-tailed Chi-square).

Supplementary Figure 5. Searchable dendrogram of co-varying arch genes.

Click here to Download Figure 5

Supplementary Table 1. Additional information about the dorsoventral gene list.

	Gene Name	Description	Arch expression pattern
Ventral			
hand2	*heart and neural crest derivatives expressed 2*	Transcription factor	Ventral (Miller et al., 2000)
sema3bl	*sema domain, immunoglobulin domain (Ig), short basic domain, secreted, (semaphorin) 3bl*		Validated here
fzd9b	*frizzled class receptor 9b*	G-protein coupled receptor	Validated here
foxf2a	*forkhead box F2a*	Transcription factor	Validated here
dcps	*decapping enzyme, scavenger*	Hydrolase of Histidine triad (HIT) family	Not tested
smad6a	*SMAD family member 6a*	Bmp signaling pathway transducer	Validated here
cep57l1	*centrosomal protein 57, like 1*	Centrosomal protein	Not tested
foxf1	*forkhead box F1*	Transcription factor	Validated here
skp2	*S-phase kinase-associated protein 2*	Ubiquitin protein ligase	Validated here
crabp2b	*cellular retinoic acid binding protein 2, b*	Retinoic acid binding protein	Ventral (Sharma et al., 2005)
pitx1	*paired-like homeodomain 1*	Transcription factor	Validated here
twist1b	*twist family bHLH transcription factor 1b*	Transcription factor	Validated here
LRRN3	*leucine rich repeat neuronal 3*	Transmembrane protein	Not tested
sumo3b	*small ubiquitin-like modifier 3b*	Polypeptide similar to ubiquitin	Not tested
barx1	*BARX homeobox 1*	Transcription factor	Dorsal and ventral (Barske et al., 2016)
Ventral-Intermediate			
fgfbp2a	*fibroblast growth factor binding protein 2a*	Fgf binding protein	Validated here
dlx4b	*distal-less homeobox 4b*	Transcription factor	Ventral- intermediate (Talbot et al., 2010)
dlx3b	*distal-less homeobox 3b*	Transcription factor	Ventral- intermediate (Talbot et al., 2010)
si:dkey-16p21.8			Not tested
hoxa2b	*homeobox A2b*	Transcription factor	Arch-wide (Hunter and Prince, 2002)
shox	*short stature homeobox*	Transcription factor	Ventral- intermediate (Sawada et al., 2015)
dlx5a	*distal-less homeobox 5a*	Transcription factor	Ventral- intermediate (Talbot et al., 2010)
gsc	*goosecoid*	Transcription factor	Ventral and Dorsal (Miller et al., 2000)
tmem107l	*transmembrane protein 107*		Validated here
stmn1a	*stathmin 1a*	Oncoprotein	Validated here
si:ch211-222l21.1			Not tested
CABZ01110379.1	*twisted gastrulation BMP signaling modulator 1b, twsg1b*	Regulator of Bmp signaling	Not tested
her6	*hairy-related 6*	Notch-dependent transcription factor	Validated here
msxe	*muscle segment homeobox 1a*	Transcription factor	Ventral-intermediate (Zuniga et al., 2011)
si:ch211-282k23.2			Not tested
otud4	*OTU deubiquitinase 4*	Regulator of DNA alkylation repair	Not tested
hoxb2a	*homeobox B2a*	Transcription factor	Arch-wide (Hunter and Prince, 2002)
ift22	*intraflagellar transport 22*	Intraflagellar transport particle protein	Not tested
dlx1a	*distal-less homeobox 1a*	Transcription factor	Ventral-intermediate (Sperber et al., 2008)
id3	*inhibitor of DNA binding 3*	Transcriptional regulator	Not tested

	Gene Name	Description	Arch expression pattern
tmem119b	*transmembrane protein 119b*		Not tested
AL929378.1	*SRY (sex determining region Y)-box 11a, sox11a*	Transcription factor	Not tested
Intermediate			
emx2	*empty spiracles homeobox 2*	Transcription factor	Validated here
irx7	*iroquois homeobox 7*	Transcription factor	Intermediate (Askary et al., 2015)
si:ch7a-166c6.1			Not tested
fsta	*follistatin a*	Activin/Bmp antagonist	Validated here
zgc:162612			Not tested
igfbp5b	*insulin-like growth factor binding protein 5b*	Secreted protein modulating tissue distribution of IGF	Validated here
ctgfb	*connective tissue growth factor b*	Secreted protein regulating Vegf, Tgf-β and Bmp signaling	Validated here
grem2b	*gremlin 2, DAN family BMP antagonist b*	Bmp antagonist	Intermediate (Zuniga et al., 2011)
ms4a17a.11	*membrane-spanning 4-domains, subfamily A, member 17A.11*		Not tested
foxd1	*forkhead box D1*	Transcription factor	Validated here
nkx3.2	*NK3 homeobox 2 (bapx1)*	Transcription factor	Intermediate (Miller et al., 2003)
dlx4a	*distal-less homeobox 4a*	Transcription factor	Ventral-intermediate (Talbot et al., 2010)
spon2b	*spondin 2b, extracellular matrix protein*	Extracellular matrix protein	Not tested
si:dkeyp-3b12.10			Not tested
si:dkeyp-3b12.8			Not tested
rgmd	*RGM domain family, member D*	Activator of Bmp signaling pathway	Not tested
Dorsal			
pou3f3a	*POU class 3 homeobox 3a*	Transcription factor	Validated here
prss35	*protease, serine, 35*	Serine proteases	Not tested
fmoda	*fibromodulin a*	Interstitial proteoglycan interacts with collagen type I and II	Not tested
si:dkeyp-3b12.6			Not tested
sfrp2	*secreted frizzled-related protein 2*	Modulator of Wnt signaling	Validated here
kera	*keratocan*	Cornea-specific keratan sulfate proteoglycan	Not tested
emp2	*epithelial membrane protein 2*	Regulator of cell membrane composition	Not tested
calhm2	*calcium homeostasis modulator 2*	Cation channel activity	Not tested
cdh11	*cadherin 11*	Membrane proteins mediating cell-cell adhesion	Validated here
pou3f3b	*POU class 3 homeobox 3b*	Transcription factor	Validated here
gata3	*GATA binding protein 3*	transcription factor	Maxillary (Sheehan-Rooney et al., 2013)
serpinf1	*serpin peptidase inhibitor, clade F, member1*	Secreted collagen-binding glycoprotein	Not tested
ednraa	*endothelin receptor type Aa*	G-protein coupled receptor mediating Edn1 signaling	Dorsal (Nair et al., 2007)
emilin1a	*lastin microfibril interfacer 1a*	Extracellular matrix protein	Not tested
postnb	*periostin, osteoblast specific factor b*	Cell adhesion molecule	Validated here
cd248a	*endosialin a*	Transmembrane glycoprotein	Validated here
arl4ca	*ADP-ribosylation factor-like 4Ca*	Small GTPase	Not tested
jag1b	*jagged 1b*	Notch ligand	Dorsal (Zuniga et al., 2010)
zfp36l1b	*zinc finger protein 36, C3H type-like 1b*		Not tested
thbs1b	*thrombospondin 1b*	Matrix protein	Not tested

	Gene Name	Description	Arch expression pattern
s1pr3a	*sphingosine-1-phosphate receptor 3a*	G-protein coupled receptor	Not tested
rassf10a	*Ras association domain family (N-terminal) member 10a*	Ras effector	Validated here
wu:fu92b05			Not tested
osr2	*odd-skipped related transciption factor 2*	Transcription factor	Frontonasal and maxillary (Swartz et al., 2011)
TRIL	*TLR4 interactor with leucine-rich repeats*	Component of toll-like receptor 4 signaling complex	Not tested
cxcl12b	*Chemokine ligand 12b*	Ligand of chemokine signaling	Ventral (Hess and Boehm, 2012)
dse	*dermatan sulfate epimerase*	Epimerase	Not tested
mn1a	*meningioma 1a*	Protooncogene	Not tested
bmp2b	*bone morphogenetic protein 2b*	Ligand of bmp signaling	Oral ectoderm (Swartz et al., 2011)
kctd15a	*potassium channel tetramerization domain containing 15a*	Adaptors for Cullin E3 ubiquitin ligases	Dorsal (Dutta and Dawid, 2010)

Supplementary Table 2. TALEN/CRISPR target sites and genotyping conditions.

Gene	TALEN/CRISPR target site	Mutation type	Genotyping primers (5'-3')	Restriction enzyme
cd248a	GGCTACCATCAGACATCCAA	11-bp deletion induces frameshift after aa 63 (of 719)	F: GCAATGAGGATGGGTGCTAT R: CGTCTTGAAGCCAGTTTGTG	BccI
ctgfa	GGACACCTGTGGGTGCTGCC	10-bp deletion induces frameshift after aa 52 (of 345)	F: GCTCAAGAGTGCAGTGGACA R: GCCAAGATCCTTACCTGTGC	HpaII
cdh11	L: TTAAATACATCCTTTCAGGG; R: TTGTCATCGATGACAAATAT	4-bp deletion induces frameshift after aa 104 (of 800)	F: ATAGGCAGCACCCACAGTTC R: TGCATGAGGAACAAGCTGTC	BfuAI
ctgfb	GGAGCCATGCGACCATCATA	4-bp deletion induces frameshift after aa 70 (of 347)	F: GACGAGAGCCCATTATGTCC R: AAAATGTTTGGGCTACCTTTCA	BccI
emx2	L: TTAGTGTTCGCTGAGGCTGT; R: TGAATGGACTGGGACGGCGG	10-bp deletion induces frameshift after aa 74 (of 247)	F: ACTATGTTTCAACCCACACCG R: TTGCGAAAAGAGGGTGCG	BtsCI
fsta	GGTGGATGATCTTCAATGGC	14-bp deletion induces frameshift after aa 84 (of 322)	F: GGTAACTGCTGGCTTCAA R: TCATTCAATACTGACGGGA	AciI
fstb	GAATGAGTGTGCCCTCCTTA	14-bp deletion induces frameshift after aa 142 (of 344)	F: GGTGGCTGATCTTCAATGGT R: TTTGCATTTTCCCTGGTACTG	Bsu36I
her6	L: TGCCGATATCATGGAAAAAA; R: TGCTCGCCGGAGTCGCGGCG	8-bp deletion induces frameshift after aa 10 (of 270)	F: GCGTACTTGACAGCGTTTACT R: CAAGCTTTCGTTGATTCTCGC	EarI
mrrf	GGAGGATATTATCAGCCTGG	4-bp deletion induces frameshift after aa 78 (of 257)	F: AAGGGCAGACAGCTAAAG R: ATAACTGTGGCTTCAGGTT	EcoNI
sfrp2	I: GGTGCAGAAACAGTGTCATC; II: GGCCGGACATGCTGGACTGC	161-bp deletion induces frameshift after aa 85 (of 249)	F: AAACATGCGTCTGCCTAACC R: AAATGAATTGATCGCGCATT	n/a
osr1	L: TGCCTGGCCTGGTGGATGCC; R: TGGGGGAACAGTGGGATTGA	7-bp deletion induces frameshift after aa 80 (of 264)	F: GGCGAACTATTCTTTCCTTCAGACC R: GGTTTACTTTTGCTGGATGCTCC	EarI
osr2	L: TGGACGGTGGGCTTCCCGCA; R: TGCGCCGGGGAAGCGCGGGT	23-bp deletion induces frameshift after aa 57 (of 238)	F: ACACTGAACGCGTTCCCG R: GATTGGCGAAGTCGAAGCG	BstNI

TALEN pairs (L,R) were used to generate mutants for *cdh11*, *emx2*, *her6*, *osr1*, and *osr2*. CRISPR gRNAs were used to generate mutants for *cd248a*, *ctgfa*, *ctgfb*, *fsta*, *fstb*, *mrrf*, and *sfrp2*. For *sfrp2*, two gRNAs were used to make a larger deletion of the coding region.

Supplementary Table 3. Cloning and synthesis of in situ probes.

Gene	Forward cloning primer (5'-3')	Reverse cloning primer (5'-3')	Enzymes
cd248a	CCTCTTGACTTCCCTGGAGA	GCGAACCTCATGAAACACAA	BamHI, T7
cdh11	TGATGAACAACCCCATCAGA	GCTAATACGACTCACTATAGGTGTTCTCC CGAATGTCTTCC	EcoRI, T7
ctgfb	GGCTACACCCCATTCTGCTA	GGCATCCAGACAACTCGAAA	EcoRV, Sp6
emx2	AACTGGAGGAAGAAGGGTCG	AAAACACTATAACGCAGCACTG	PstI, Sp6
fgf20b	CAGCTATGGGAGAGATCGGG	GGTCCACAGGTCTTGGAAGA	EcoRV, Sp6
fgfbp2a	TGTGGACAATCTCAAGCACAC	TGACGAAGGAGCATGCACTA	BamHI, T7
fgfbp2b	AGTCCATTACACCTTCGCCA	ACTGATTGACTCTCCTCCGC	BamHI, T7
foxd1	GAGATCCTGCTCAACGGTTC	GGACTTAGAGGGGGGTAGAA	EcoRI, T7
foxf1	GATCGTATCAGGGCTGGAAA	TGTCACACATGCTGGGAGAT	EcoRI, T7
foxf2a	GTCACTACTGGACCATAGAT	AGAGAATACGGAGGCATACT	BamHI, T7
fsta	GGAAGACCAGGAGGATGACGATG	TCCGTTGACCTTGTGTTCGC	EcoRV, Sp6
fzd9b	TATCATCCGATCAGTCGCCG	TACGGTGCATCCCAGATGAGG	NotI, Sp6
her6	ACCAGTTGAACTCGGGACAC	TTGAACCATGGGTTGACTGA	EcoRI, T7
igfbp5b	GCTGGGTACATTTCTGACGG	TGGATGTTACCGCCACTGTA	EcoRV, Sp6
kctd15a	GCACTCTCACGCTTCAACAA	AATAACATGGGTCGGGTCCT	PstI, Sp6
mrrf	GTTCCCAAGGTAACTCGTG	TCGTTGTTCACCCTGTGTG	SpeI, T7
osr2	CAGCTCAACTACTCGCTCCTG	ATTGAGGGGTGAGTGTGTCC	BamHI, T7
pitx1	CCCGAAGAAGAAGAAGCAGC	TATGCTCGTCTCTGCTCCAG	BamHI, T7
postnb	AGTGACCCGAGTTATCCAGG	GTTTAAGGCATCTGTTCCCTGC	HindIII, T7
pou3f3a	AAACAAACTTCCATGCACAATG	GTGCCCGAGTGTAGGTCTTC	EcoRV, Sp6
pou3f3b	GCATTCTTTTGCCCCCTAC	TCATCTCTTACGGAATCACTACTGAAA	BamHI, T7
rassf10a	CAGGAAAAACAGCGGAGGATTG	CCCAAACATTGTCTACTGAAGGCAG	NotI, Sp6
sema3bl	TGCTGTTTGGCTCGAGATCC	GTCTACTGTGAGGCGATGCG	EcoRV, Sp6
sfrp2	TACAAACCTGCTCCTGTGCC	TGAAGTTTGCGAATGCTGCG	HindIII, T7
shox	AACAGCAGGAGTGATCTAAACCC	TCTTGCCTTGAGTCGCAGGTCA	EcoRV, Sp6
skp2	GACATCTGGGACTGAGCCG	TCCATCAGGTCAAGGTATACTGC	HindIII, T7
smad6a	TATGTCTCCCTCCTCGCTGG	TCATTTGGGGGTTAGTCGTGG	HindIII, T7
snai1a	AGCTTGCTACCTTCCCTTCA	ACCCTACCATAGTCAACCCAC	EcoRV, Sp6
stmn1a	GTGAGAAAACGGCGCGAGG	ACACAAGTCCCCACCAAGTCC	NotI, Sp6
tmem107l	AATGTCGGTGGTCAGCAGTCTG	GAGTTTATTGTGCCAGTGAGTGAATG	EcoRV, Sp6
twist1b	CTCCCTCCTCTCAAACACTTT	GCACACTAGTGAGATGCAGAC	BamHI, T7

Restriction enzymes and type of RNA polymerase for synthesis are shown in the last column.

Table S4. TPM values for all RNA sequencing experiments.

Click here to Download Table S4

Table S5. TPM values and filtering of dorsoventral gene list.

Click here to Download Table S5

Supplementary References

Dutta, S. and Dawid, I. B. (2010). Kctd15 inhibits neural crest formation by attenuating Wnt/beta-catenin signaling output. *Development* **137**, 3013-3018.
Hess, I. and Boehm, T. (2012). Intravital imaging of thymopoiesis reveals dynamic lympho-epithelial interactions. *Immunity* **36**, 298-309.
Miller, C. T., Yelon, D., Stainier, D. Y. and Kimmel, C. B. (2003). Two endothelin 1 effectors, hand2 and bapx1, pattern ventral pharyngeal cartilage and the jaw joint. *Development* **130**, 1353-1365.
Miller, C. T., Schilling, T. F., Lee, K., Parker, J. and Kimmel, C. B. (2000). sucker encodes a zebrafish Endothelin-1 required for ventral pharyngeal arch development. *Development* **127**, 3815-3828.
Nair, S., Li, W., Cornell, R. and Schilling, T. F. (2007). Requirements for Endothelin type-A receptors and Endothelin-1 signaling in the facial ectoderm for the patterning of skeletogenic neural crest cells in zebrafish. *Development* **134**, 335-345.
Sawada, R., Kamei, H., Hakuno, F., Takahashi, S. and Shimizu, T. (2015). In vivo loss of function study reveals the short stature homeobox-containing (shox) gene plays indispensable roles in early embryonic growth and bone formation in zebrafish. *Dev Dyn* **244**, 146-156.
Sharma, M. K., Saxena, V., Liu, R. Z., Thisse, C., Thisse, B., Denovan-Wright, E. M. and Wright, J. M. (2005). Differential expression of the duplicated cellular retinoic acid-binding protein 2 genes (crabp2a and crabp2b) during zebrafish embryonic development. *Gene Expr Patterns* **5**, 371-379.